

Review

# The Design of a Thermoelectric Generator and Its Medical Applications

Palanisamy Mohan Kumar <sup>1,\*</sup>, Veluru Jagadeesh Babu <sup>2</sup>, Arjun Subramanian <sup>1,2</sup>,  
Aishwarya Bandla <sup>3</sup>, Nitish Thakor <sup>3,4</sup>, Seeram Ramakrishna <sup>1</sup> and He Wei <sup>2</sup>

<sup>1</sup> Centre for Nanofibers and Nanotechnology, Department of Mechanical Engineering, National University of Singapore, Engineering Drive 3, Singapore 117587, Singapore; arjun.subramanian@u.nus.edu (A.S.); seeram@nus.edu.sg (S.R.)

<sup>2</sup> Singapore Institute of Manufacturing Technology, Surface Technology group, ASTAR, Fusionopolis way 2, Innovis, Singapore 138634, Singapore; babu@simtech.a-star.edu.sg (V.J.B.); hewei@simtech.a-star.edu.sg (H.W.)

<sup>3</sup> Singapore Institute for Neurotechnology (SINAPSE), National University of Singapore, 28 Medical Drive, Singapore 117456, Singapore; aishwarya.bandla@nus.edu.sg (A.B.); eletnv@nus.edu.sg (N.T.)

<sup>4</sup> Department of Biomedical Engineering, Johns Hopkins University, Baltimore, MD 21218, USA

\* Correspondence: mohan@nus.edu.sg

Received: 21 March 2019; Accepted: 23 April 2019; Published: 26 April 2019



**Abstract:** Growing energy demands are driving people to generate power in every possible way. New energy sources are needed to plug the energy gap. There is a growing interest in distributed energy generation due to its remarkable advantages such as flexibility, reliability, adaptability and minimal transmission losses. Thermoelectric generators (TEGs) are one such distributed power source that relies on thermal energy for electricity generation. The current review focusses on the design and optimization of TEGs to maximize the power output from the available thermal sources. The basic principle of thermoelectricity generation and suitable architecture for specific applications are explained with an overview of materials and manufacturing processes. Various cooling techniques to dissipate heat from the cold side and their influence on overall efficiency are reviewed in this work. Applications of TEGs for powering biomedical sensors have been discussed in detail. Recent advancements in TEGs for various implantable devices and their power requirements are evaluated. The exploitation of TEGs to generate power for wearable sensors has been presented, along with published experimental data. It is envisioned that this study will provide profound knowledge on TEG design for specific applications, which will be helpful for future endeavours.

**Keywords:** thermoelectric; generator; Peltier; cooling; heating; thermal management; wearable; sensor; body heat; implantable

## 1. Introduction

Thermoelectric devices (TEDs) were conventionally used for thermal management as early as 1950 [1], when they were first conceived. Being compact, lightweight and with no moving parts, they offer a unique cooling solution replacing bulky compressor-based refrigeration, despite their lower efficiency [2]. The ability of TEDs to heat and cool offers precise temperature control for temperature-sensitive environments. Most of the studies on TEDs focus on the development of materials [3] and associated system components towards enhancing the system-level efficiency, which is comparatively low (~5%) [4] compared to compressor-based refrigeration (40-50%) [5]. With the exponential growth of energy demands, decentralized power generation is more lucrative compared to conventional fossil fuel-based generation. Reliable, flexible and adaptable distributed power sources

are always in demand. TEDs are realized to generate electricity by converting thermal energy, apart from their conventional use as cold sinks. This unique power generation widened its usage from space exploration [6] to powering micro-biomedical sensors. TEDs meant for power generation are referred to as thermoelectric generators (TEGs) and thermoelectric coolers (TECs). The advancements in thermoelectric materials boost the efficiency of thermal-to-electric conversion, enhancing their commercial potential. TEGs are known for the following remarkable advantages, despite the low thermal to electric conversion efficiency:

- High reliability with no moving parts; maintenance-free
- Wide range of power generation (kW– $\mu$ W)
- Noiseless operation
- Compact size and can be embedded in an existing setup
- Direct energy conversion without any intermediate form of energy conversion.

However, the power generation efficiency of TEGs depends on the material, the system-level components and their arrangement. Hence, the current review encompasses the design of TEGs and their associated components starting with an introduction to the working principle of TEGs, followed by materials and applicable manufacturing processes. The architecture of TEGs and their commercial applications are discussed in detail. A section has been dedicated to the presentation of various cooling techniques to maintain the cold side temperature of TEGs and assess their impact on power generation. An exhaustive review is presented on the medical application of TEGs, especially on the implantable and wearable devices. The portable health care devices market is expected to grow in the coming decades, fuelling research into TEDs with a higher coefficient of performance (COP).

## 2. Working Principle of Thermoelectric Devices

TEDs work on the principle that electric potential and heat can be seamlessly converted. The Seebeck effect states that electric potential can be generated between two junctions at different temperatures if the circuit is formed with two dissimilar metals. The Peltier effect, which is the reverse of the Seebeck effect, insists that the temperature can be controlled between two junctions if electric potential is applied between two dissimilar metals. TEDs use the Seebeck effect in power generation mode and the Peltier effect in thermal management mode, as shown in Figure 1. This versatility of TEDs is attractive for niche applications such as precise temperature control [7]. A TED consists of a large number of thermocouples formed by n-type and p-type semiconductor materials connected electrically in series and thermally in parallel. A thermoelectric module (TEM) generally consists of heat sinks on both hot and cold sides with interface and insulating layers to prevent heat diffusion to the cold side. It is obvious that the efficiency of the module is the sum of the efficiency of each element that forms the module, as shown in Figure 1. The conversion efficiency depends on the figure of merit  $\overline{ZT}$  (Average value of  $ZT$ ), as given by Equation (1). A higher value of  $ZT$  is preferred for the power generation and it was concluded by Bell [8] that  $ZT > 1.5$  is substantial for waste heat recovery applications. During the early period of development, the  $ZT$  value was mostly less than 1, but due to the advancement of materials a  $ZT$  of 2–3 is reported. The  $ZT$  values of different powers sources are displayed in Figure 2 [9]. For a given TEM, the maximum heat-to-electric conversion efficiency is given by Equation (2) and is proportional to the temperature of the hot, cold side and figure of merit  $ZT$  [9]. The variation of  $ZT$  values and corresponding efficiency is given in Figure 2. As a cooling device, the cooling efficiency is characterized by the COP as expressed in Equation (3):

$$ZT = \frac{\alpha^2}{R.K} \times (T) \quad (1)$$

$$\eta_{TE} = \left( \frac{T_{Hot} - T_{Cold}}{T_{Hot}} \right) \left( \frac{\sqrt{1 + \overline{ZT}} - 1}{\sqrt{1 + \overline{ZT}} + \frac{T_{Cold}}{T_{Hot}}} \right) \quad (2)$$

$$COP_{max} = \left( \frac{T_{Cold}}{T_{Hot} - T_{Cold}} \right) \left( \frac{\sqrt{1 + \overline{ZT}} - \frac{T_{Hot}}{T_{Cold}}}{\sqrt{1 + \overline{ZT}} + 1} \right) \quad (3)$$

where  $\alpha$ ,  $R$ ,  $K$ , and  $T$  are the Seebeck coefficient, electrical resistance, thermal conductance, and absolute temperature, respectively. A higher value of  $ZT$  is desirable for both cooling and power generation applications.

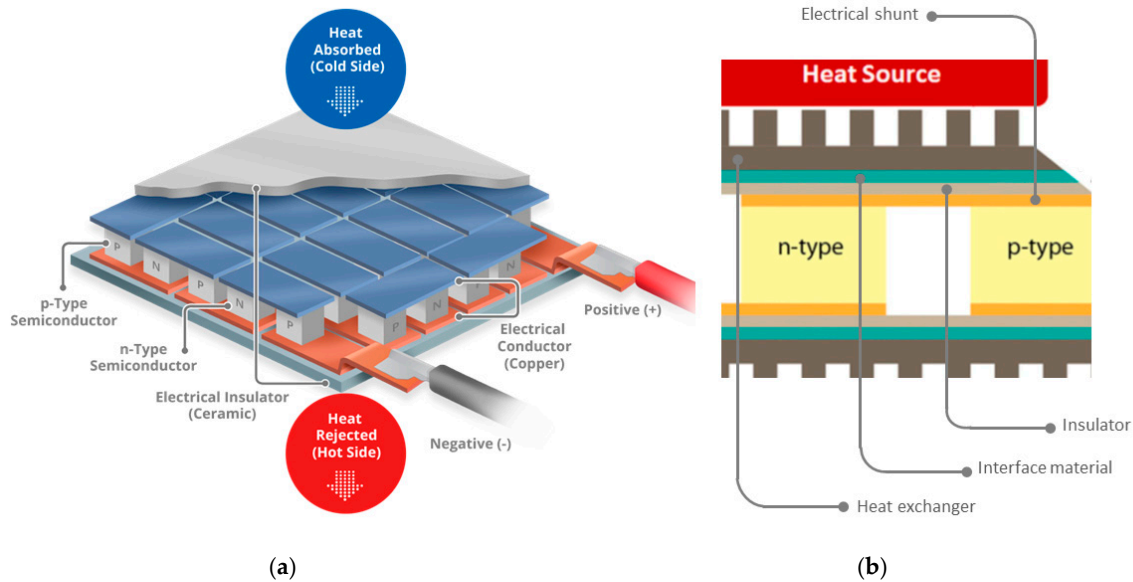


Figure 1. (a) Working principle of TEG and TEC; (b) components of a typical thermoelectric generator.

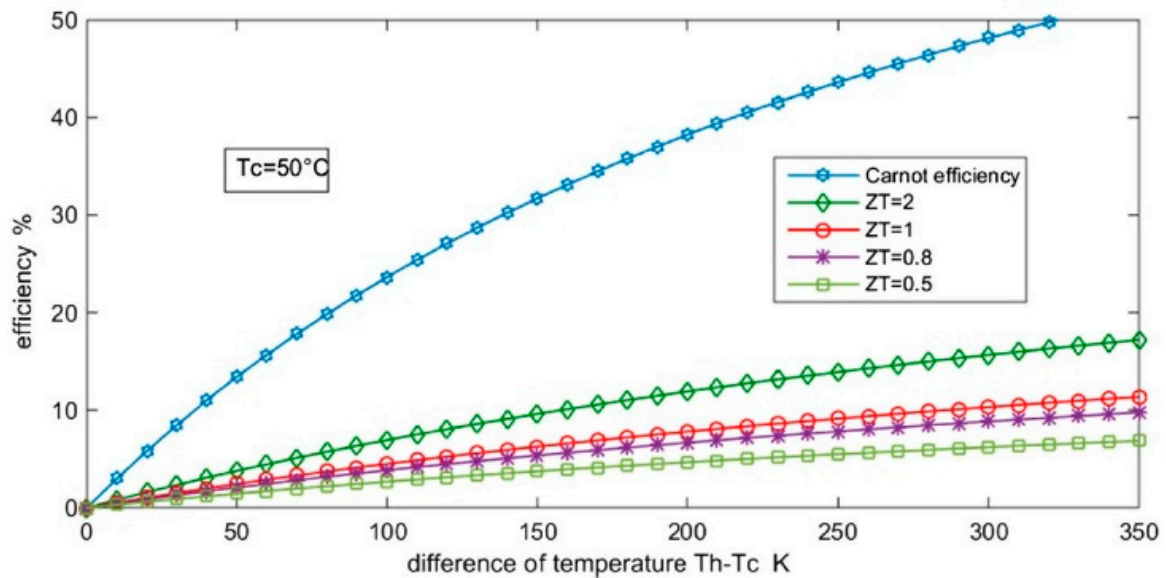


Figure 2. Variation of TEM efficiency for different  $ZT$  [9].

### 3. Materials and Manufacturing Process of TEG

This section presents a short overview of thermoelectric materials and their manufacturing process with cost considerations. Readers who are interested in the materials and manufacturing process are directed to the literature for information on thermoelectric materials [10], bulk thermoelectric materials [9], and low-dimensional thermoelectric materials [11]. The primary objective of thermoelectric material research is to achieve a high value of  $ZT$  [12], characterized by a high Seebeck coefficient, low thermal conductivity [13] and high electrical conductivity. It is an immense

challenge for researchers to optimize these conflicting parameters together with the desired mechanical properties. In the past, thermoelectric materials were mostly bulk alloy materials such as SiGe, CoSb<sub>3</sub>, Bi<sub>2</sub>Te<sub>3</sub> and PbTe [14]. Based on their material structure and composition, they are categorized as half-Heusler, silicide, an oxide, clathrate, skutterudite, and chalcogenide [15]. Though chalcogenides display thermoelectric properties, the majority of commercial TEM modules are manufactured using bismuth telluride (Bi<sub>2</sub>Te<sub>3</sub>) with various additives [16]. Bi<sub>2</sub>Te<sub>3</sub> was introduced with nanomaterials [17] to reduce the lattice thermal conductivity through an enhanced phonon-scattering rate. The electron concentration is optimized by the addition of nanomaterials that act as phonon-scattering sites. The addition of such nanomaterials aids in achieving a glass-like thermal conductivity, termed phonon-glass electron-crystal (PGEC) [14], due to long mean-free path phonons increasing the transport of heat and charge. A notable increase in the value of  $ZT$  to 1.86 at 320 K was reported [18] by reducing the lattice thermal conductivity and point defect scattering. A  $ZT$  value of 2.6 at 923 K was registered by Kanatzidis [19] for Sn-Se crystals due to its ultra-low lattice thermal conductivity. Materials with a  $ZT$  value as high as 3 [10] were identified in the literature by decoupling the heat from the charge transfer.

Although intensive research on materials has significantly improved the  $ZT$  value, there are underlying challenges to employing these materials in commercial devices. It is an immense challenge to match the peak value of  $ZT$  at a single temperature, as most of the applications allow temperature fluctuations following thermal cycling [20]. Since peak  $ZT$  values occur at high temperatures above 600 °C, material stability over the operating temperature is vital from a device perspective. Even at high temperatures, the exposed thermoelectric material should not oxidize [21]. Some materials are reported to undergo sublimation [22] due to high-temperature spikes, which may lead to device malfunctions. The above issues limit the high-value  $ZT$  thermoelectric materials from transferring into commercial products. Knowledge of the mechanical properties of thermoelectric materials is imperative for device design and manufacturing, which is often hindered by peak  $ZT$  values. Thermoelectric materials are brittle [23] and it is challenging to assess material characteristics such as fracture strength, fracture toughness and hardness [24] due to changes in composition and material testing techniques [25]. TEGs operate at a wide range of temperatures as high as 600–1000 °C in cases of furnace exhaust [8] or as low as 20 °C, while generating power for implantable devices within the body. Hence the Coefficient of Thermal Expansion (CTE) is a critical parameter due to thermal cycling. As each component, shown in Figure 1, will have a different CTE, especially on the solder joints of the thermoelectric legs, significant stress may build up [26]. Attention has to be paid while selecting the interface layers, substrates and interconnects, which should be stable over a wide range of operating temperatures to prevent early device failures. CTE varies significantly among commonly studied materials such as MNiSn = 8–12 parts per million K<sup>-1</sup> (ppm) [27], Mg<sub>2</sub>Si = 3–6 ppm K<sup>-1</sup> [28], and Si-Ge alloys = 10–12 ppm K<sup>-1</sup> [29]. Proposed solutions include employing liquid metal layers [30], carbon nanotube arrays [31] and designing multiple contact layers with gradually varying CTE.

### *Manufacturing of Thermoelectric Materials*

The manufacturing process of TEGs is based on the architecture of TEGs and the thermoelectric material that is employed. The overview of manufacturing process presented here is more generic and more oriented towards to the manufacturing of flat bulk TEGs. The motive is to enlighten TEG designers on the implications of their design on the manufacturing process and the cost.

As the first step, the thermoelectric material has to be synthesized, typically through ball milling [32] along with its constituents. The steps involved in the manufacturing of TEGs are displayed in Figure 3. Though the process is extensive, the required characteristics can be achieved once the optimized material composition is established. Another process by which thermoelectric powders can be obtained is through melting [33], though there is some degree of process fluctuation resulting in a variation in phase and microstructures [34]. Synthesized powders are then formed into ingots, either by hot pressing or spark plasma sintering, and are subsequently diced to form thermoelectric legs. Material brittleness leading to chipping of thermoelectric legs is a predominant issue in this process,

which may lead to further cracking [35]. Established manufacturing processes from semiconductor industries such as etching [36], molecular beam epitaxy, electroless etching and vapour deposition [37] are employed for manufacturing thin-film TEGs. Most commercially available TEGs are manufactured using bismuth telluride, while lead telluride and germanium are rarely used. The raw material cost of  $\text{Bi}_2\text{Te}_3$  is \$110/kg [38], whereas if it is converted to pure thermoelectric material the cost is \$806/kg [38]. The development of polymers, oxides and silicide drastically reduces the need to use germanium, thereby reducing the cost of the raw materials. The raw and pure thermoelectric material costs of oxides are \$2/kg and \$50/kg [39], respectively. The cost of manufacturing TEGs varies based on the manufacturing process and the type of raw materials used. The total cost of TEG modules is also substantially shared by the components such as heat exchangers and substrates.

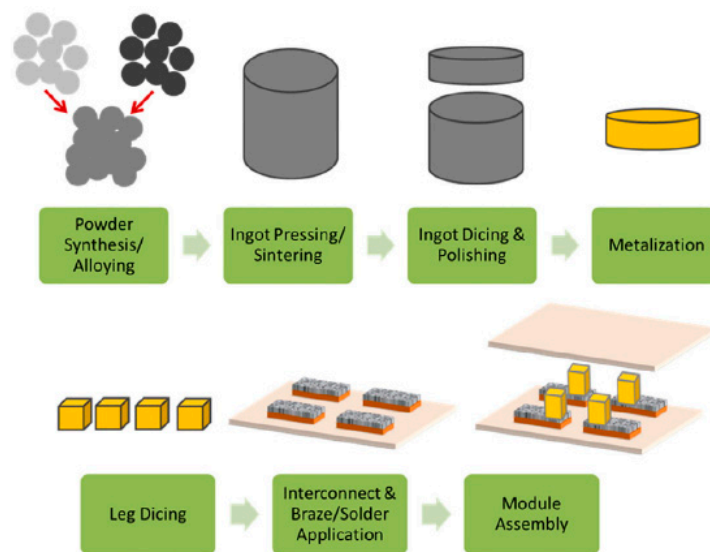


Figure 3. Typical manufacturing process of TEG [32].

#### 4. Architecture of Thermoelectric Generators

Various architectures of TEGs are employed due to various shape of the heat recovery surface in contact. The electrical, thermal and power generation characteristics are greatly influenced by the architecture of TEGs. Minimizing the heat loss and contact thermal resistance are the primary objectives of any TEG architecture, in relation to the cost considerations. Based on their architecture, the TEGs are classified as follows.

##### 4.1. Flexible TEGs

Due to the advent of flexible power electronics and wearable sensors, there is high demand for flexible power sources for applications such as powering sensors, and monitoring biomechanical motions. Flexible architectures of TEGs provide such flexibility without compromising the efficiency compared to rigid TEGs. Flexible TEGs employ novel polymers, composites, and are fabricated through innovative manufacturing methods such as additive manufacturing, printing, thermal spraying instead of conventional subtractive manufacturing. Polymers such as polyaniline exhibit good thermoelectric (TE) properties, which can be further optimized with conductive additives such as carbon nanotubes (CNT) with Au nanoparticles. A planar TEG was fabricated by doping a polyethyleneimine (PEI) solution onto CNT, demonstrating a power factor of up to  $10^{-3} \text{ W/m}^{-1} \text{ K}^{-2}$  [40]. Printable and paintable TEGs are reported to adhere to various geometries. Research is ongoing to formulate suitable inks that have adequate wettability, viscosity and binder materials. A combination of organic and inorganic binders shows good electrical transport [41]. Rollup TEGs consisting of metal films coated on a polyamide roll by using an inject printer were demonstrated by Weber [42]. A special type of TEG

known as Origami, which is flexible enough to be pasted on heat sinks, has the potential to replace batteries [43], as shown in Figure 4.

Another study introduces a method to fabricate a TEG from a hybrid thermoelectric material [1] made by granulating carbon nanotubes into p/n-type bismuth telluride (Bi/Te) and distributing this mixture within a highly flexible material polydimethyl siloxane (PDMS) [44]. This hybrid thermoelectric material was processed into pillar shapes as shown in Figure 4 [7], followed by selective etching of the PDMS to reduce contact resistance between interconnects and the fabricated thermoelectric material.

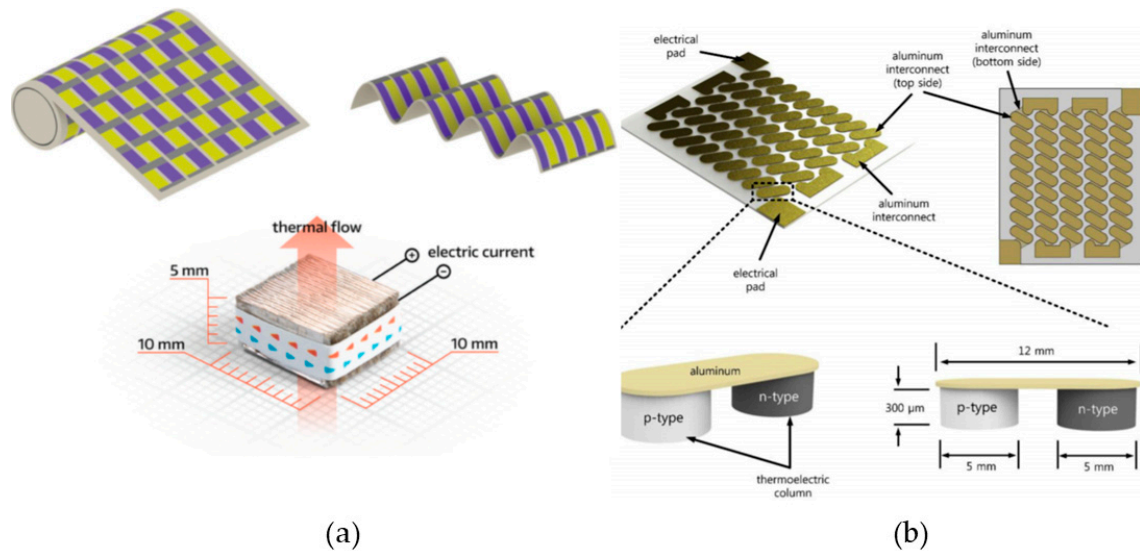


**Figure 4.** (a) Processing of a flexible origami TEG; (b) flexible thermoelectric generator with polydimethyl siloxane [43].

#### 4.2. Cylindrical Bulk TEG

Cylindrical bulk TEGs are suitable to extract power from cylindrical objects such as cooling channels and automotive exhaust pipes where the heat flows radially. Cylindrical bulk TEGs are fabricated by using PbTe modules through a sintering process [45]. Manufacturing of ring-shaped TE materials with high homogeneity and density is a challenge. Long tubes of PbTe modules are made from p-type and n-type TE doped with PbTe and cut into the required lengths. The TE legs are separated by insulation rings and alternatively connected by inner and outer metallic tubes, as shown in Figure 5 [46]. The cartridge configuration shown in Figure 5 was developed for automotive applications and is optimized to operate with exhaust gas on the hot side and a water-glycol mix on the cold side. The heat exchangers customized for exhaust gas pipes operate in the temperature range of 400–650 °C on the hot side and coolant (water-glycol) in the temperature range of 40–100 °C. The thermoelectric elements are p-type and n-type, with their legs hermetically enclosed in inert gas. The enclosure, consisting of a heat exchanger on the outer hot surface and a cooling tube on the inner cold surface of the cartridge, is illustrated in Figure 6. The cartridge was assembled on a SUV-BMW X3 (BMW AG, Research and Innovation Center: Munich, Germany) [47] to generate power in the range of 0.5 to 2 kW. The electrical power obtained from this four-ring prototype is 30 mW when a temperature difference of 70 K is maintained across the inner and outer surfaces of the thermoelectric tube [46].

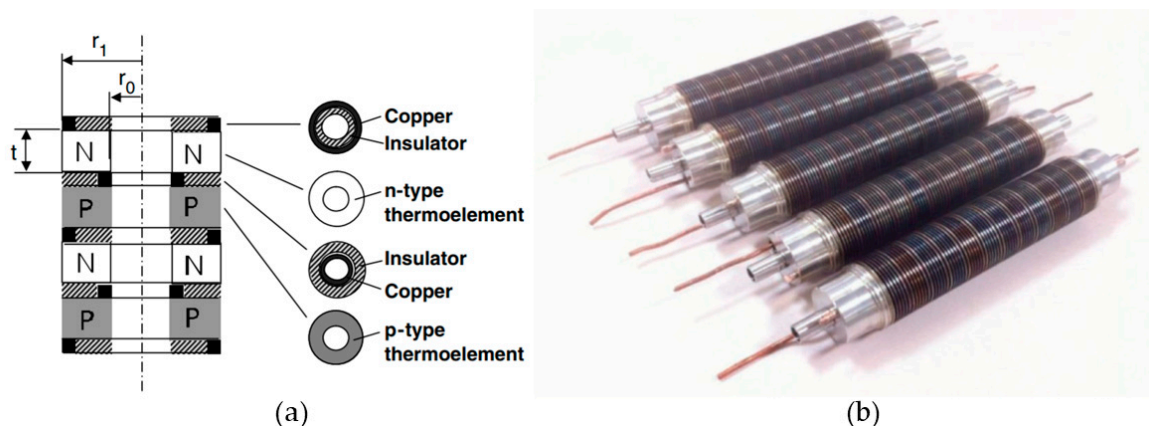


Figure 5. (a) Components of ring shaped TEG; (b) cylindrical cartridge TEG for exhaust gas pipe [45].

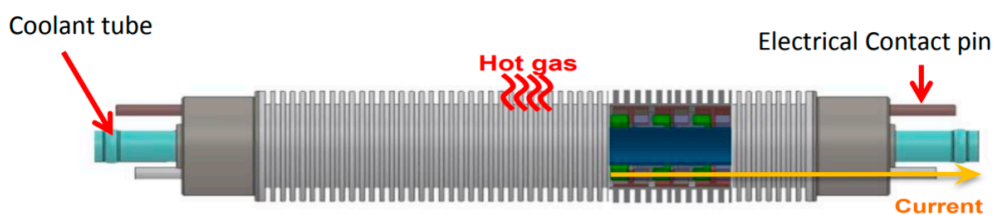


Figure 6. Typical cylindrical TEG for an automotive exhaust showing the stacked TE elements, with inner and outer fins as heat exchangers [46].

### 4.3. Flat Bulk TEG

Flat bulk architecture TEGs are widely employed for high power generation to exploit the longitudinal Seebeck effect [48]. The flat bulk TEGs are mostly cuboid in shape, with electrical and thermal current running parallel to each other. The flat bulk TEGs are constructed with alternating legs of p-type and n-type TEM by a powder processing or sintering technique. Metallization layers are constructed on both sides of the legs with highly thermal conductive materials such as alumina ( $Al_2O_3$ ) or aluminium nitride based on the cost. Extensive studies are in progress to enhance the performance of flat bulk TEGs through geometric factors and TE legs arrangement [49]. TEGs with square or pyramidal TE legs are illustrated in Figure 7. The effect of the number of TE legs and their dimensions was studied by Hodes [50]. The shapes of TE legs such as pyramidal, cuboid or quadratic were studied by Mijangos [51]. TEGs with pyramidal TE legs are found to generate 70% more power than cuboid ones. The flat bulk TEGs are used in waste heat recovery and concentrated solar radiation applications. Flat bulk TEGs have been used in experiments in the automotive field and generated up to 1 kW [52] from waste heat. The use of TEGs in concentrated solar radiation can greatly reduce surface contact loss such as heat loss and thermal contact resistance. Studies on the photo thermoelectric effect open up new areas of application

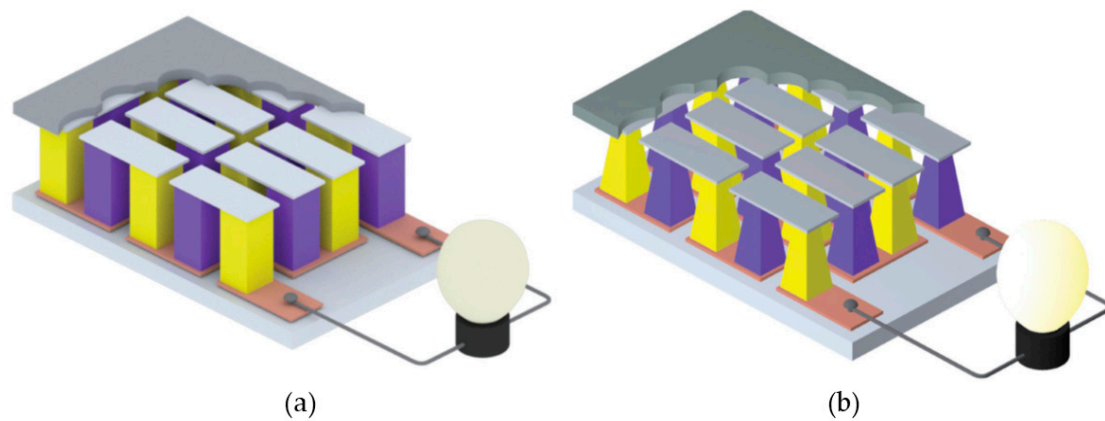


Figure 7. (a) Flat bulk TEG with n-type, p-type square legs; (b) flat bulk TEG with pyramidal legs [48].

#### 4.4. Thin-Film TEG

Thin-film TEGs are typically designed in the thickness range of a few micrometres, hence high densities of cooling power are attainable due to the high heat flux. Electrochemical deposition is identified as a more suitable method, as well as economical to fabricate thin-film TEGs as compared to sputtering. A micro-TEG consisting of 126 TE legs of n-type and p-type  $(\text{Bi, Sb})_2\text{Te}_3$  obtained by electrochemical deposition was produced by Snyder [53]. High internal resistances on the order of  $\text{M}\Omega$  [54] and complex fabrication technologies [55] are intrinsic problems of micro-TEG devices.

### 5. Cooling of Thermoelectric Generators

As TEGs exploit the temperature difference between their two sides, maintaining a higher temperature difference will help with increasing the power yield. The hot side of the TEG is in thermal contact with a heat source such as a waste heat pipe or concentrated solar radiation, while the cold side temperature is kept low by cooling it to the maximum possible extent. The widely employed cooling methods of TEGs, and their classifications, are shown in Figure 8. All the heat that is incident on the hot side will not be converted into electricity, as a vast amount of heat ends up heating the device. To maintain the temperature difference, the heat that is diffused from the hot side must be dissipated from the cold side. Significant studies in the past have contributed to the hot side thermal management [56], whereas cold side thermal management has not received sufficient attention. Since designing a successful TEG involves choosing the right cooling method based on factors such as TEG size, amount of heat flux, cost and space availability, this section has been dedicated to providing an overview of cooling mechanisms and their impact on the power generation of TEG.

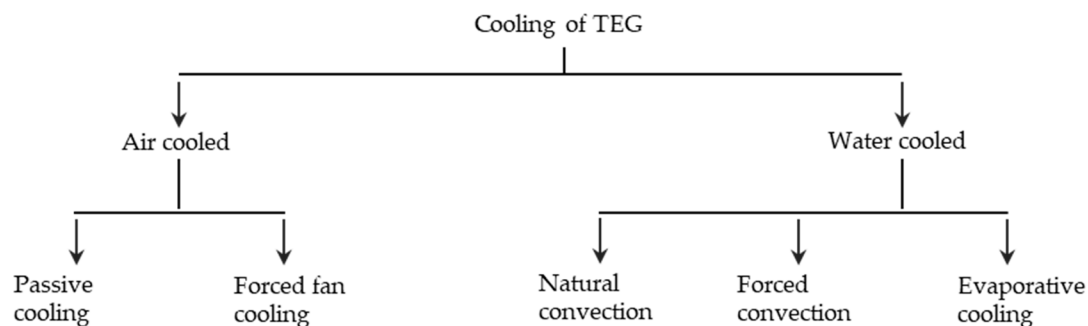


Figure 8. Schematic of an evaporative cooling system for TEG.

The efficiency of increasing the cold side temperature for various  $ZT$  is shown in Figure 2. It was experimentally reported that for every  $50\text{ }^\circ\text{C}$  rise in the cold temperature, the efficiency drops by 3.5%, while the hot side temperature was maintained at  $1030\text{ }^\circ\text{C}$  [57]. Studies on solar TEGs (STEG) reveal

that the electrical production drops from 1.62% to 1.25% when the cold side temperature rises from 5 °C to 150 °C [57]. Theoretical predictions indicate that the efficiency of the TEGs can be improved by 5–10% by choosing the right cooling method and temperature [58].

### 5.1. Air Cooling

#### 5.1.1. Passive Air Cooling

Passive cooling involves dissipating heat from the cold side to air through natural convection. In the study by Özdemir [59] on STEGs, the efficiency is comparatively low when cooled by an isolated wind chimney. For a temperature variation of 10 °C inside the chimney, the cold side temperature increases from 30 °C to 77 °C. The study was extended to compare the efficiency when the cold side temperature is fixed at 30 °C. Though a peak efficiency of 6% was achieved, the average efficiency hovers around 3%. A similar experimental investigation performed by [60] revealed that the output increases with an enhanced fin design.

#### 5.1.2. Forced Air Cooling

Forced air cooling is the simplest cooling method compared to other methods, which typically use a fan of the required capacity. Wilson [61] reported power generation of 4 W using a 1 W fan on a smaller TEG. The advantage of a fan-cooled system is that it is adaptable to various sizes of TEGs and environments. An added advantage is the use of air and its availability. The efficiency of the forced air cooling relies not only on the mass flow rate of the air; heat sink design and the nature of the forced air also significantly affect the cooling rate. Different configurations of heat sinks have been investigated by Hsu [62] to find the optimum number of fins. Peak efficiency of 2.1% was achieved, generating 44.1 W at a temperature difference of 88.3 K. A comparative study [63] of various convection methods versus the individual leg length,  $L$ , and the results are shown in Figure 9.

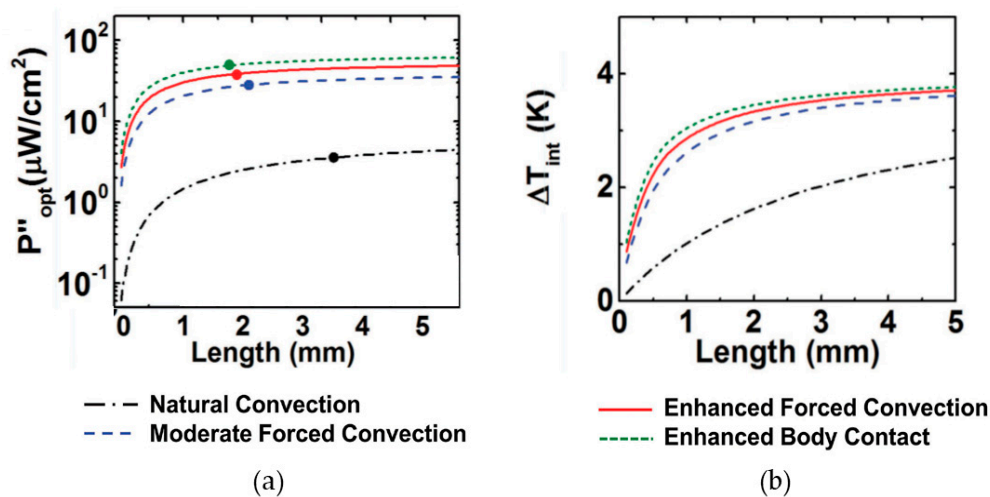


**Figure 9.** (a) Power output comparison of different cooling methods for different leg lengths; (b) temperature difference for different lengths [63].

#### 5.1.3. Water Cooling

Water cooling is by far the most widely adapted cooling method in most thermal systems, and TEG is no exception [64]. The high heat capacity of water and its abundant availability make it more attractive. Although a substantial amount of power will be used to move the water, this parasitic loss will be accounted for when defining the total efficiency of the device. STEG with a parabolic dish using water cooling can reach an efficiency of 2.81% [65].

#### 5.1.4. Natural Convection

Compared to forced convection, natural convection is not preferred due to the larger size and low rate of heat rejection. The experimental study by Champier [66] employs an aluminium tank filled with water on the cold side of the TEG, while the exhaust air from the biomass stove is in contact with the hot side through aluminium fins. Maximum power of 9.5 W was generated by using domestic water as a coolant. Another similar study [67] uses an open water tank filled with water, which would evaporate as the temperature increases. A lab prototype designed by Singh [68] uses a thermosyphon on a salinity-grade solar pond, generating 3.2 W of power.

#### 5.1.5. Forced Convection

Forced water cooling is efficient in terms of heat extraction compared to the methods discussed above, though a significant parasitic loss does exist when delivering water at the required flow rate. Various operating parameters such as hot and cold side temperatures, flow rate and convection efficiency were studied by Niu [69]. The maximum efficiency of 4.44% at the power output of 146.5 W was achieved with a coolant at 30 °C. In the case of STEG, forced water cooling was researched extensively. A microchannel heat sink was designed to cool the individual thermopiles and was able to generate 4.9 W at electrical efficiency of 2.9% when the temperature difference was 109 °C [64]. Yazawa [70] was able to achieve 1% convection efficiency by using ambient water and a Fresnel lens. Most studies on STEG use a parabolic concentrator and forced water cooling, and on average they are able to generate 64.8 W of power at 1.59% efficiency [71]. Advances in computational fluid dynamics, together with sophisticated computer models, are able to predict the total system efficiency, as indicated by Aranguren [72]. Heat transfer also depends on the type of heat exchanger design. A comparative study of the tube and fin heat exchanger reveals that the fin exchanger design performs better, especially at low Reynolds number flows [73]. The exchanger designs are shown in Figure 10. Further investigation is required on system design including optimization of pumps, coolant, flow rate, heat exchanger design and piping to reduce parasitic loss.

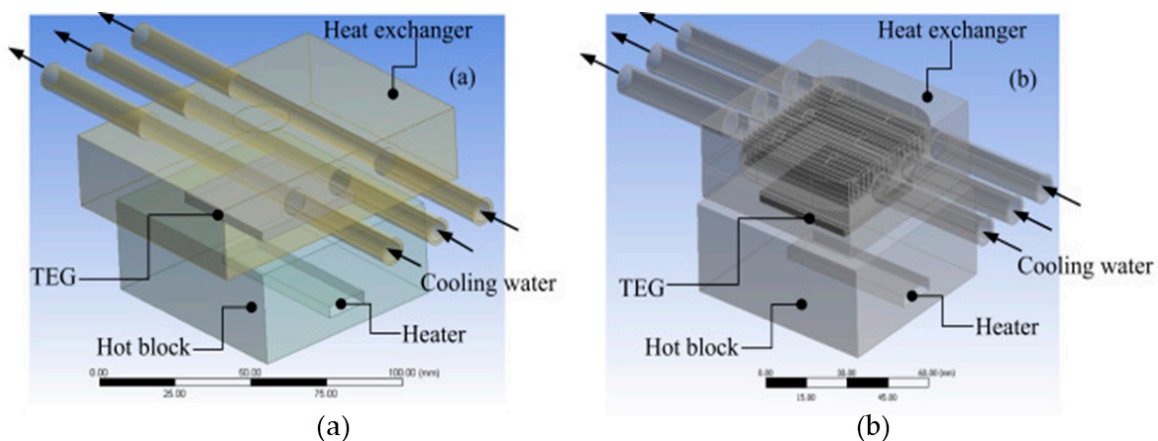


Figure 10. (a) Tube heat exchanger; (b) fin heat exchanger [71].

#### 5.1.6. Evaporative Cooling

Evaporative cooling utilizes the latent heat of vaporization of water in conjunction with heat pipes. Maximum heat flux was achieved with this type of cooling in comparison with the above discussed cooling methods. The system is more reliable due to the heat pipe design. A closed-loop design of heating pipes was realized by Hamade [74], generating 3 W for a temperature difference of 80 °C, while achieving a higher efficiency of 2.02%. The experimental setup using heat pipes on both the hot and cold sides is shown in Figure 11. A four- to six-fold increase in the power output was reported by Djafar [75]. Past research on STEGs involving evaporative cooling by using heat pipes demonstrated a

thermal efficiency of 40–45%, and electrical efficiency of 1% [76]. The performance of TEGs with an evaporative cooling system is influenced by the water flow pattern. The flow can be either parallel or in the opposite direction. Experiments [77] show that the counter flow pattern leads to higher output power compared to the parallel flow pattern. This can be attributed to the temperature difference between the hot gas and cooling air along the flow direction. For the parallel flow pattern, the hot gas temperature decreases, and the cooling air temperature increases along the same direction. Evaporative cooling also finds applications in the automotive industry [78], with the potential to replace radiators.

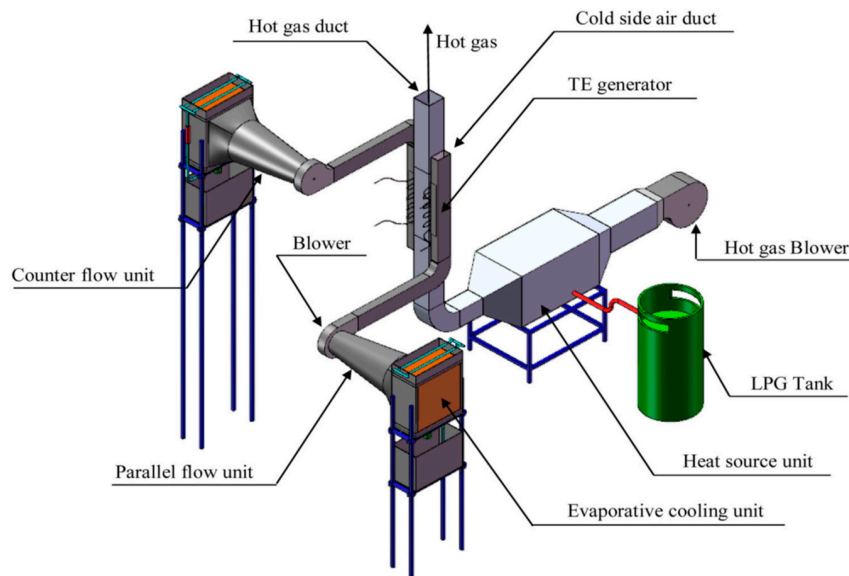


Figure 11. Schematic of an evaporative cooling system for TEG [77].

### 6. Medical Applications of Thermoelectric Generators

TEDs have been widely used in the past for temperature management of patients and medical devices, where reliability and noiseless operation are of higher importance than COP. TEDs are increasingly replacing devices that once relied on refrigeration cooling, based on a vapour compression cycle. Ultra-small sensors and next-generation wearable devices, along with the Medical Internet of Things (MIoT) [79], have positioned TEGs as primary micro energy harvesters. This section reviews the role of TEGs in wearable and implantable applications, typical power requirements of sensors, available energy harvesting techniques, and design of TEGs for such applications. The application of TEGs in medical applications can be broadly classified as shown in Figure 12.

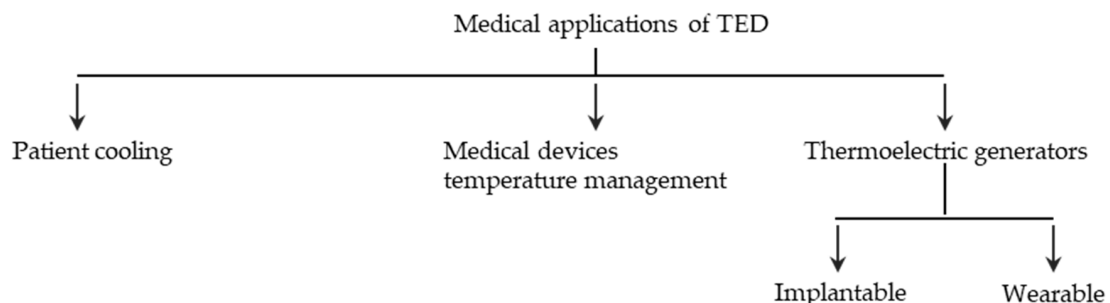


Figure 12. Classification of TED in medical applications.

Energy harvesting is categorized according to the energy sources. These include, but are not limited to, vibration/motion energy, thermal energy, solar energy, optical energy, wind energy and radio frequency (RF) radiation energy. The environment and the required power will decide the suitable energy harvesting method. Implantable devices date back to 1958 [80], with the discovery

of the implantable pacemaker for regulating abnormal heartbeats. The success of pacemakers paved the way for other implantable devices such as implantable insulin pumps to deliver insulin into the body depending on the blood sugar level of the diabetic patients [81]. Later, implantable cardioverter-defibrillators were developed for detecting cardiac arrhythmia and correcting through electric pulses [82]. Though early biomedical implants were designed to impart certain functions, the recent energy-hungry implants are equipped with wireless sensors that not only monitor and activate signals in the local region, but also collect data and send it back through wireless channels to the data storage cloud [83]. Neural implants that capture brain activity for a brain-machine interface require power to perform electrical stimulation, data capture and wireless communication, and demand significant amount of power. The required power level may vary from  $\mu\text{W}$  to  $\text{mW}$  [84], as indicated in Table 1.

**Table 1.** Power requirements of common implantable devices.

Implanted Device.	Applications	Typical Power Requirement
Cardiac pacemaker	Conduction disorders	30–100 $\mu\text{W}$
Cardiac defibrillator	Ventricular tachycardia	30–100 $\mu\text{W}$ (Idle)
Neurological stimulator	Essential tremor	30 $\mu\text{W}$ to several $\text{mW}$
Drug pump	Spasticity	100 $\mu\text{W}$ –2 $\text{mW}$
Cochlear implant	Auditory assistance	Up to 10 $\text{mW}$
Glucose monitor	Diabetes care	>10 $\mu\text{W}$

The implantable devices can be powered from either “inside the body” or “outside of the body.” The “inside the body” power sources refer to harnessing power from sources such as a thermal gradient, biofuel cell or blood glucose. The “outside of the body” power sources refer to energy from body motion, skin thermal gradient and so on.

6.1. Thermoelectric Generators for Implantable Medical Devices

TEGs are expected to play a key role in a growing number of implantable devices. This section investigates the feasibility of embedding a TEG into the human body, in vitro and in vivo experiments and their results, limitations, and future prospects. Implantable devices substitute for certain functional organs of the body and have to be in operation for the lifetime of the patient. These devices can be powered either by storing electricity or generating it on site. Some common implantable devices are shown in Figure 13 [85].

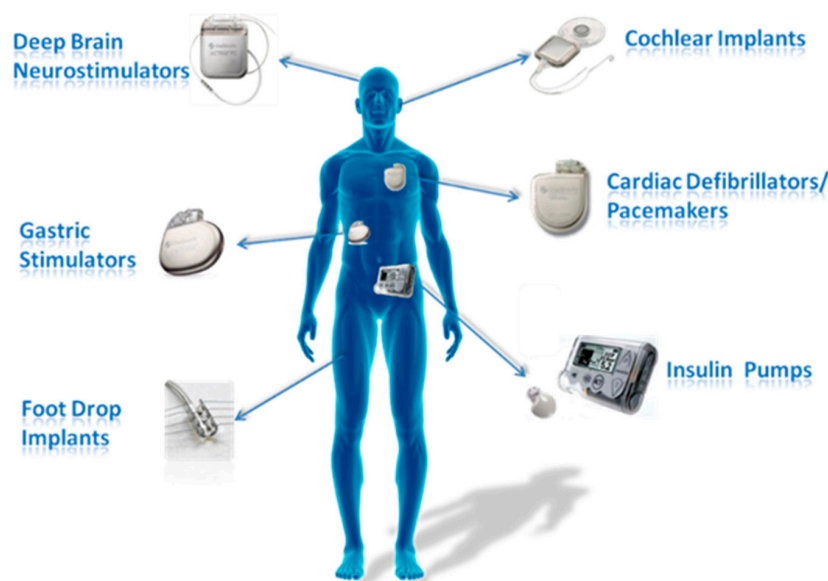


**Figure 13.** Common implantable devices.

Energy storage is accomplished through a battery. Currently, the power source for implantable devices is dominated by batteries, which have limitations in terms of safety, power density and service life. As battery technology has evolved, invoking higher power density [86], the service life of the battery has reduced significantly [87]. The problem of battery replacement is compounded by the reliability and improved device technology. Currently, lithium batteries are a widely used power source for most implantable devices due to their stability, high voltage and higher power density. Though the life span of a lithium battery is promised to be more than 10 years, recent findings in battery chemistry indicate a shortened life [88] due to increased power density, demanding frequent battery replacement. Some batteries for neurological stimulation need to be replaced in a few months, leaving patients with scars and pain. High power-requiring devices such as mechanical heart pumps are not viable for implantation but are powered through a wearable battery in the waist.

### 6.1.1. Design of TEGs for Implantable Devices.

TEGs are one possible means of achieving power generation for implantable devices. Achieving the required power is the first step in designing a TEG. From Table 1, the maximum power requirement can be approximated as 100  $\mu$ W for most of the devices. Since TEGs generate power through the temperature difference, it is necessary that a sufficient temperature gradient exists in the human body. In order to maximize the power generation from the TEGs, they should be located at the part of the body where the temperature gradient is highest. The core body temperature is regulated at 37  $^{\circ}$ C [89], while a higher temperature gradient is available on the skin surface [90], where it radiates heat to the environment. Hence, the skin surface and the layers of tissues and their temperature distribution have to be fully understood. A simplified model of human tissues with embedded TEG is shown in Figure 14.

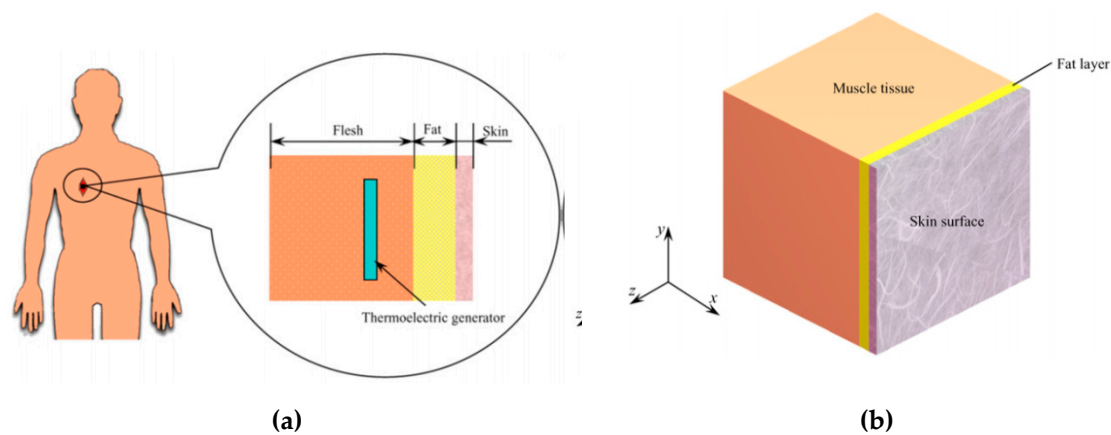


**Figure 14.** (a) TEG embedded in three-layer human tissue; (b) cubic domain of human tissue [90].

The voltage generated across the junction of TEG can be obtained through Equation (4):

$$V_{output} = n \times \Delta T (\alpha_1 - \alpha_2), \tag{4}$$

where  $V_{output}$  is the output voltage from the TEG,  $\Delta T$  is the temperature difference across the two junctions of the TEG,  $n$  is the number of thermocouples that are electrically connected in series, and  $\alpha_1$  and  $\alpha_2$  are the Seebeck co-efficient of TEG thermoelements, respectively. The temperature across the two junctions for the steady state heat transfer is given by Equation (5) for a one-dimensional heat transfer:

$$\Delta T = q \times \delta / k_t, \tag{5}$$

where  $q$  is the heat flux arriving at the hot junction from the interior tissue side, and  $\delta, k_t$  denote the thickness and thermal conductivity of the TEG, respectively. The heat transfer through the body tissues can be derived through the Pennes bioheat formulation [91], as given in Equation (6):

$$\rho c \cdot \frac{\partial T(x, t)}{\partial t} = \nabla k(x) \nabla [T(x, t)] + Q_b + Q_m, \tag{6}$$

where  $T(x, t)$  is the tissue temperature distribution and  $k(x)$  the space-dependent thermal conductivity of the tissue.  $\rho_b, c_b$  are the density and specific heat of the tissue, respectively.

$$Q_b = \rho_b c_b \omega_b(x) (T_a - T(x, t)), \tag{7}$$

where  $\omega_b(x)$  is the space-dependent blood perfusion. Past studies indicated that a temperature gradient of 1-5 K [92] exists but varies significantly depending on the TEG position in the body. It is apparent that the higher the blood perfusion and the metabolism heat generation rate, the higher the temperature gradient, which is favourable for power generation through TEG. Additionally, within the fat layer there is a temperature difference due to the lower thermal conductivity reported by Ishida [93]. Temperature gradient of 4-5 K was derived by using the parameters listed in Table 2 in the abdominal region.

**Table 2.** Material properties and convective heat transfer coefficients used for tissue thermal modelling.

Material	Thermal Conductivity	Density	Heat Capacity
Muscle	0.7–1.0 W/m K	1070 kg/m <sup>3</sup>	3471 J/kg K
Fat	0.1–0.4 W/m K	937 kg/m <sup>3</sup>	3258 J/kg K
Skin	0.5–2.8 W/m K	—	—
Blood	0.51–0.53 W/m K	1060 kg/m <sup>3</sup>	3889 J/kg K

The study also indicated that an obese person has a higher thermal gradient due to thick layers of fat and being able to generate higher power through the TEG. With a 5 K temperature difference and 100  $\mu$ W at 1 V power requirement, the size of the TEG can be calculated with Bi<sub>2</sub>Te<sub>3</sub> TEG. TEG with 1000 thermocouples is required for 1 V, as the voltage output is proportional to the number of thermocouples. Output voltage is also influenced by element spacing and material properties, resulting in a TEG of 1.3 cm<sup>2</sup>.

An in vitro study has been conducted with a pork fillet of size 80 mm  $\times$  80 mm to simulate the human body with fat layer of thickness 10 mm and skin layer of thickness 2 mm. The constant heat source is a copper plate at 310 K with thermostat and ambient temperature of 291 K. A TEG was embedded with cold side interfacing between fat and muscle tissue as depicted in Figure 15. It was found that when the temperature difference is 0.5 K after stabilization, the output voltage of a single TEG is 3.3 mV. As shown in Figure 15b, the start of cooling indicates the time when a piece of ice is placed to increase the temperature gradient to 1.1 K, resulting in a TEG output of 6 mV. Though this experiment sheds some light on the capability of TEGs, an important factor of thermoregulation by the body has not yet been accounted for. Hence, an in vivo study will give a realistic output of TEG. A single TEG was embedded inside a rabbit weighing 3.2 kg, as shown in Figure 16. As the TEG output was unstable, it was connected to a booster circuit with a DC/DC converter. The output of the TEG and the voltage generated are shown in Figure 17. The in vitro study concluded that a functional circuit, booster circuit is essential, along with a thermocouple array (TEG), to power an implantable device.

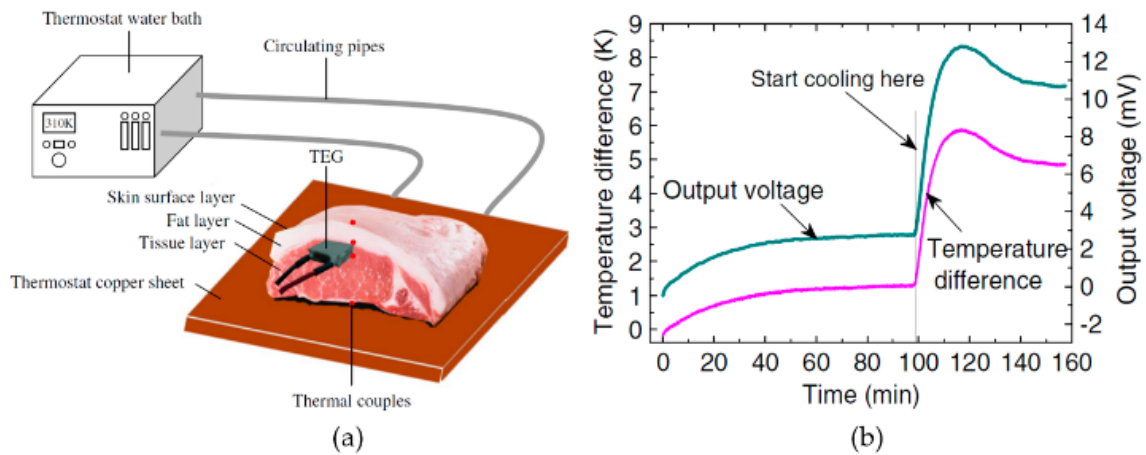


Figure 15. (a) In vitro experimental setup; (b) output voltage in relation to temperature difference [90].

The above experiments reveal that embedding a TEG into the human body to power the implantable devices is feasible; our conclusions are as follows:

- The TEG can be located at an implantable depth from the skin surface, where the maximum temperature difference exists.
- Multi-stage TEG can generate higher power for the same temperature difference compared to single TEG.
- Skin cooling and higher ambient temperature will enhance the TEG output.
- As the voltage output from the TEG is not sufficient since the implantable device impedance is 0.5 to 100 kΩ [94], the commercially available thermoelectric module's figure of merit has to be significantly increased.
- The TEG should be covered with high thermal conductivity and a biocompatible membrane before implanting it into the human body.

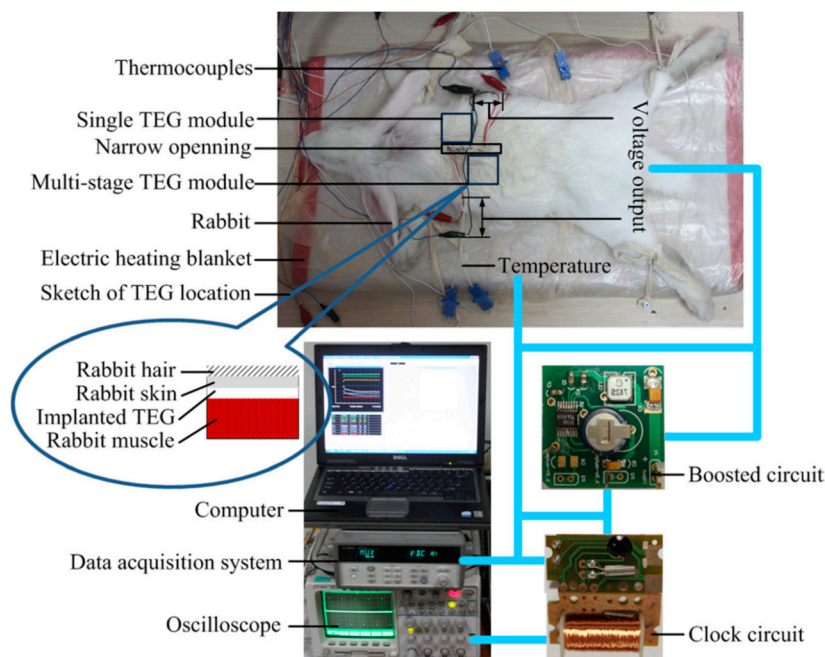
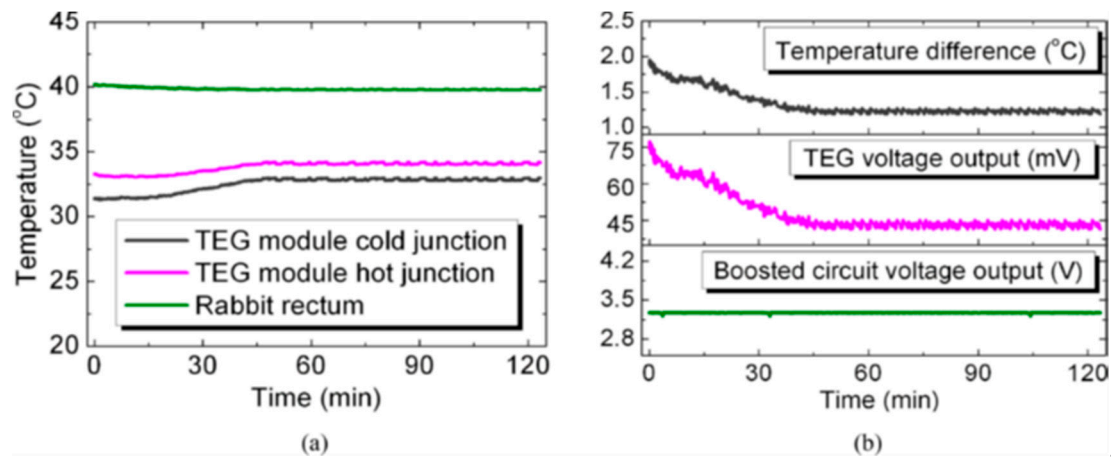


Figure 16. In vivo experimental setup with a rabbit [94].



**Figure 17.** (a) Temperature profile of TEG and rabbit rectum; (b) output voltage in relation to temperature difference [94].

### 6.1.2. Pacemaker

The heart is a vital part of the human body and any interruption or abnormalities in its operation can cause cardiac arrest and eventually death. The heart ceases to function due to a malfunction of the sino-atrial node (SA node) [95] that disrupts the electrical conduction system. Currently, pacemakers that can generate electrical pulses to control the heart rhythms employ batteries that can last for a maximum of 10 years [96]. The depleted battery has to be surgically replaced with a new battery. As an alternative, active research has been ongoing to convert body heat to electrical energy by using TEGs. A feasibility study [97] has been conducted by employing 4000 thermocouples in series of a size of about 6.0 cm<sup>2</sup>, generating 4 V for a 1 °C temperature difference. The basic charging circuit is shown in Figure 18 along with the PN junction array for the pacemaker. The primary function of the charging circuit is to monitor the voltage level from the TEG and cut off if it is above the threshold voltage by using a Timer IC NE555. Control voltage pin 5 of IC<sub>1</sub> is provided with a reference voltage of 5.6 V by Zener diode. Battery charging through TEG follows a three-stage charging algorithm [98]. The charging process starts with the pre-charge stage; once the battery voltage reaches a certain point, it switches to the bulk charge stage, followed by the absorption stage. When the charger is disconnected from the power line, it automatically switches off within 1 min. The study estimates that the pacemaker life can be extended by more than 30 years by continuously charging with a temperature difference of 2 °C.

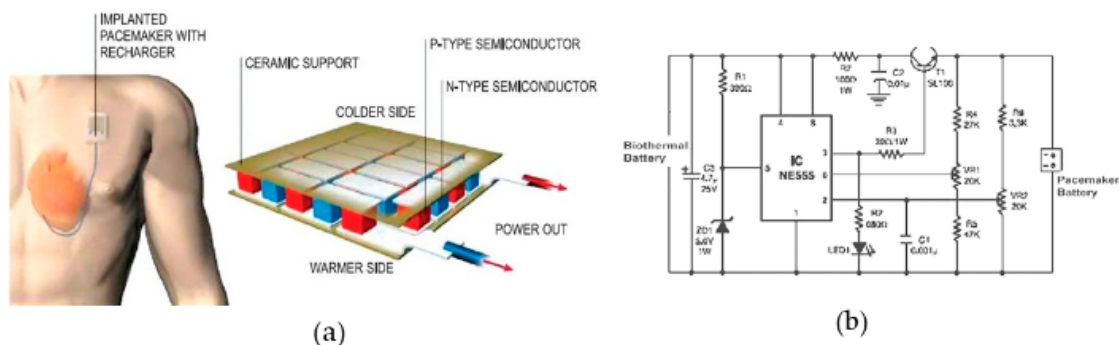


**Figure 18.** (a) P-N junction array for pacemaker; (b) battery charging circuit [98].

### 6.2. Wearable Healthcare Devices

The importance of low-cost sensors is growing, especially for patient health monitoring. Wearable health monitoring devices provide real-time data to assess a patient’s condition over a period of time. Notable success has been achieved when powering these devices through a patient’s body

movements [99], yet a solid-state device can transmit the data without any interruption. These sensors with low sampling rate demand low power [100], which is made possible by harnessing the energy from the human body. The possibility of powering these body sensors through wearable TEG is due to a significant reduction in the sensor size and low-power transmission systems. The wireless transmission power requirements have been reduced drastically to  $\sim 10 \mu\text{W}$  [101].

Widely used body sensors include electroencephalography (EEG) for measuring neural activity at the scalp, electrocardiography (ECG or EKG) for measuring cardiac activity, electromyography (EMG) for recording electrical activity of the muscles, and pulse oximeters to monitor the blood oxygen saturation and patient pulse. Though the diagnostic purpose of a sensor and the measuring parameters may vary, the principle of operation is the same. All these sensors measure the electrical pulse from the tissues by measuring the body ion flow. This is accomplished by applying electrolytic gel (Cl<sup>-</sup>) ions with Ag to initiate a chemical reaction resulting in a 10–100  $\mu\text{W}$  electrical signal [102]. These signals are amplified and transmitted wirelessly to an IoT gateway, which will store these data in the cloud. With the explosive growth in Artificial Intelligence (AI), these data may yield valuable conclusions regarding patients' health, thereby reducing the need for a doctor's intervention. Currently available remote monitoring vests are listed in Table 3 with their power requirements. These vests transmit data through Bluetooth and are powered by batteries.

**Table 3.** Remote monitoring vests and their power requirements.

Model	Manufacturer	Ref
Health Vest	Smart Life Technologies	[103]
Vital Sense.	Philips-Respironics	[104]
Life Shirt	Vivo Metrics	[105]
Equivital	Bio-Lynx Scientific Equipment, Inc.	[106]
Bioharness	Zephyr	[107]
ProeTEX	Curone	[108]
ExMedicus Smartwatch	Planet Intelligent	[106]

The human body functions like a thermostat set at 37 °C at the core, while the skin temperature is variable. Heat is generated in the body based on metabolic activity and is dissipated to the surroundings primarily by convection and evaporation [109]. The metabolic activity varies based on the physical activity and age, yet the designed TEG should be able to generate the required power with the minimal metabolic rate. Since wearable TEGs are placed on the skin, in order to increase the heat flux, a heat sink or radiator [110] can be employed, as shown in Figure 19, though the size is limited. It is shown that the heat flux from the skin can double for a heat sink the size of a wristwatch. Due to the high thermal resistance of the body, the heat flux from the skin is curtailed, even with an efficient heat sink. Determining the thermal resistance of the body is a complex task, as it depends on various parameters such as proximity to arteries, vasodilation, vasoconstriction and the clothes worn. Also, attention should be paid to the heat fin design so as not to alter the body heat flow, which may lead to a sensation of discomfort.

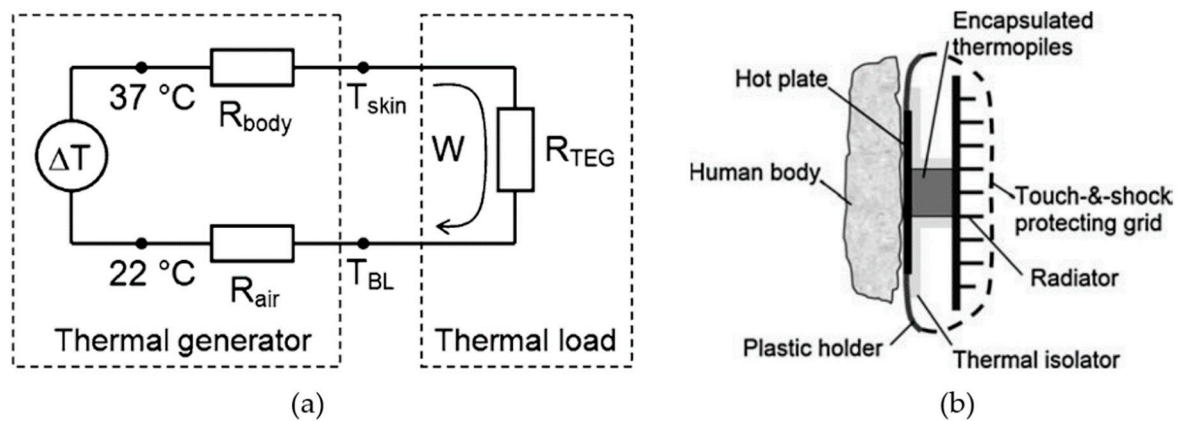


Figure 19. (a) Thermal circuit with generator and load; (b) TEG with radiator [110].

### 6.2.1. Design of a Wearable TEG

The thermal circuit of the TEG placed on the skin is displayed in Figure 19. The core body temperature is 37 °C, while the ambient temperature is assumed to be 22 °C. The heat flow  $W$  and the temperature drop on the TEG,  $\Delta T_{TEG}$  is given by Equations (8) and (9), respectively.  $R$  indicates the resistance and  $T$  indicates the temperature of the respective elements indicated with the suffixes:

$$W = (T_{core} - T_{air}) / (R_{body} + R_{air} + R_{TEG}) \tag{8}$$

$$\Delta T_{TEG} = (T_{skin} - T_{BL}) = R_{TEG} (T_{core} - T_{air}) / (R_{body} + R_{air} + R_{TEG}). \tag{9}$$

It is vital to thermally match the thermal generator (body) to the load (TEG). Due to high thermal resistance, the thermopile inside the TEG should also have high thermal resistance. Thermal matching indicates the thermal equivalent of electrical matching of generator to its load. Hence  $R_{TEG}$  can be replaced with two parallel resistance types,  $R_{tp}$ , thermopile resistance, and  $R_{par}$ , parasitic thermal resistance, as below:

$$R_{TEG,optimal} = R_{par,0} (R_{body} + R_{air}) / [2 (R_{body} + R_{air} + R_{TEG}) + R_{par,0}]. \tag{10}$$

From the above equations, considering a watch size wearable TEG, the thermal resistance is 700 cm<sup>2</sup> K/W for the temperature difference of 6–7 °C, assuming the thermal resistance of the human body is 300 cm<sup>2</sup> K/W [111]. The thermal resistance obtained at various body locations with a 3 cm × 3 cm × 3 cm TEG is listed in Table 4. As per the above formulation, a wearable TEG can generate ~300 μW/cm<sup>2</sup>. The amount of heat flow to achieve the required power will lead to discomfort. Hence, with the commercially available TEG material of  $ZT = 1$ , the maximum power generated will be ~30 μW/cm<sup>2</sup>. The measured thermal resistance on the skin with temperature variation is shown in Figure 20 [112]. The above analysis concludes with a design choice to maximize the power output from TEG by having a hot plate much larger than the thermopile and a radiator of similar size.

Table 4. Thermal resistance measurements measured at various body locations.

Body Location	Ambient Temperature °C	Thermal Resistance cm <sup>2</sup> K/W
Trunk	23	200–800
Outer wrist	22.7	440
Inner wrist	22.7	120–150
Forehead	21.5	156–380

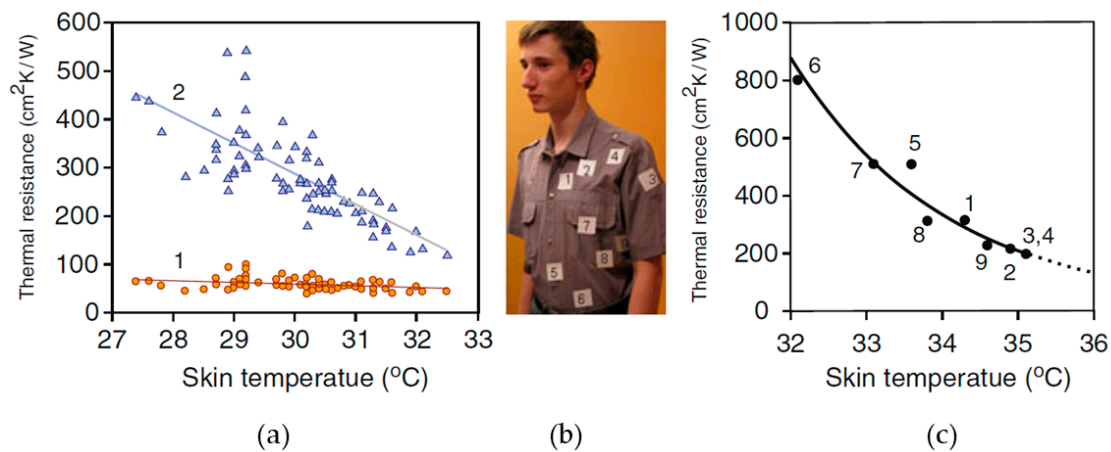


**Figure 20.** (a) Estimated thermal resistance per square centimetre of the skin, measured at  $22.7 \pm 0.5$  °C on the wrists of 77 people under the attached TEG: (1) is the thermal resistance between the body core and arterial blood in the wrist, (2) is the thermal resistance between the arterial blood and TEG. (b) Nine locations where the thermal resistance of the human body has been measured; (c) the thermal resistance of the human body at 23 °C depending on its location on the trunk [112].

Typically, a biomedical sensor consists of a transducer, signal amplifier, microcontroller, wireless transmitter and power source. It is obvious that the power required is proportional to the amount of data collected over a period of time (sampling frequency). For most sensors, the power required to function is often low and a major share is consumed when transmitting the data, substantially limiting the lifetime of the sensor. Despite an extended battery life, a low sampling rate will result in low data resolution. Torfs [113] demonstrated a wearable TEG whose power requirement varies from 0.6 to 1.4 mW when the sampling rate varies from 128 to 512 Hz. Recent success achieved in lowering the power consumption to 10 μW will open up new avenues in wearable TEGs. Also, improvements in power electronics will lead to the design of biomedical sensors with the ability to operate at less than 1 V, which is a desirable factor for wearable TEGs.

### 6.2.2. Flexible Thermoelectric Generators

TEGs embedded in clothing are a potential alternative to those mechanical devices in terms of reliability, cost and comfort. Flexible TEGs are fabricated by embedding polymers that are conductive into carbon nanotube webs. For wearable TEGs, Suarez [114] noted the importance of thermal conductivity over the Seebeck coefficient and electrical resistivity of the thermoelectric material in enhancing voltage and power generation. The thermal conductivity of the filler material in the TEG has also been demonstrated to be a critical parameter affecting the performance. The study [115] employs a flexible thermal interface layer (TIL) between the TEG and the skin. For wearable TEGs, polydimethylsiloxane (PDMS) serves as a flexible insulating and supporting material for the encapsulation of rigid thermoelectric legs. The thermal conductivity of the TIL has a greater influence on the performance of the TEG. The wearable module has several n-type and p-type thermoelectric legs interconnected by copper strips both in series and parallel, and the encapsulating PDMS around the thermoelectric legs. Figure 21 shows a schematic of a wearable TEG on a human wrist. The study also compares the performance of TEGs on flat and curved surfaces with a radius R. The voltage generated by flexible TEG, evaluated both numerically and experimentally, is depicted in Figure 22. The experimental results shed light on voltage generation during body movements such as walking or standing, as the heat generated by the body is proportional to these movements. The experimental evaluation with different TIL thicknesses indicates that a TIL of less thickness and high thermal conductivity is preferred for wearable designs. The performance of the flexible TES1-12704 module for harvesting thermal energy directly from the leg, while walking or jogging, was found to be 5 to 50 μW [116].

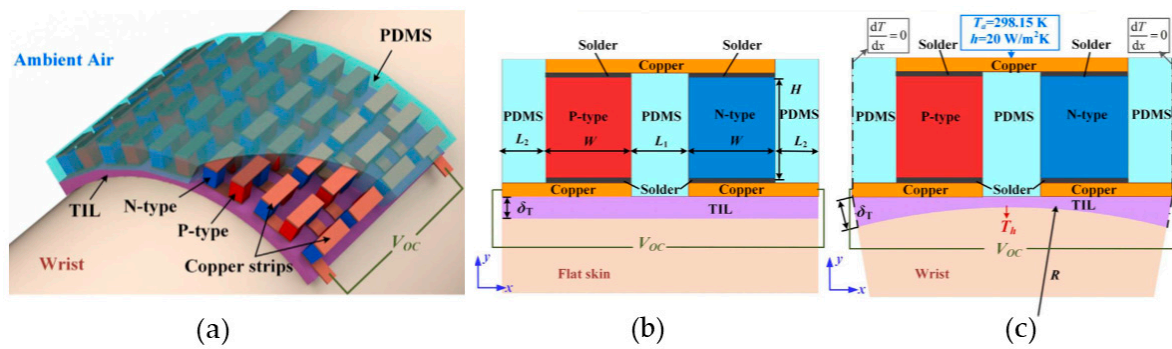


**Figure 21.** (a) Structural design of a wearable TEG on the wrist; (b) cross-sectional view of the TEG on skin that is a flat surface and (c) on skin that is a curved surface [112].

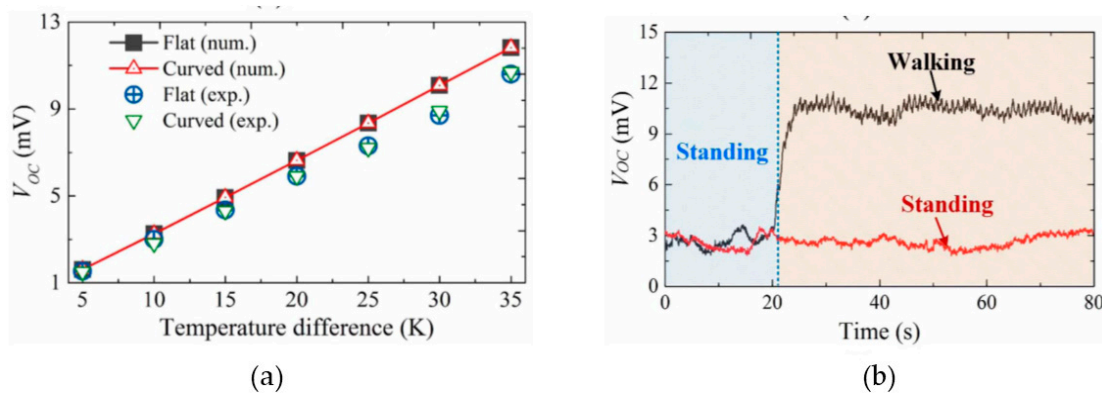


**Figure 22.** (a) Comparison of TEG voltage on flat and curved surface; (b) TEG voltage generated during walking and standing [113].

### 7. Conclusions

The present review summarizes the development of TEGs in the aspects of materials, manufacturing process, architecture, cooling methods and their applications in the medical field with an emphasis on implantable and wearable devices. The design of successful TEGs hinge on solving the coupled challenges in material development, the manufacturing process and system optimization. An overview of the working principles reveals the significance of  $ZT$  for a thermoelectric generator or thermoelectric cooler. Remarkable progress has been made in improving the  $ZT$  value to as high as 3, accomplished through continuous research on new materials along with nanomaterial additives. Even with enhanced  $ZT$  values, the remaining difficulties in achieving low thermal resistance, good thermal isolation and higher power factor are a significant challenge. Higher  $ZT$  values will undoubtedly ignite a breakthrough in various new applications that have not been imagined before.

Discussion of the material synthesis reveals the relationship between the manufacturing process and the cost. Challenges in material morphology changes, and defects due to the adoption of a semiconductor process, have been highlighted. Though materials with  $ZT$  values on the order of 3 have been demonstrated at the lab scale, significant challenges exist in industrial-scale production. selective laser sintering (SLM) is emerging as a predominant manufacturing process for thermoelectric materials, yet the flowability of power and spreading even layer by layer with constant thickness is still a major issue. Low-cost polymeric thermoelectric materials exploit well-established processes such as electrospinning and chemical vapour deposition. Substantial effort is required for tuning a manufacturing process tailored to the mass production of new nanomaterials with thermoelectric properties.

To exploit the full potential of TEGs, good knowledge of system design and performance during operation is paramount. The selection of suitable architectures is driven by geometry matching, heat sink and heat source parameters, environment and size. TEGs are optimized through the

reduction of contact thermal resistance, smaller installation space and eliminated intermediate layers through geometry matching. Predominant architectures such as flexible, cylindrical, bulk and thin-film architectures have been presented with their intended applications. Experimental studies on these TEG architectures show that the total module efficiency is enhanced through the matching of CTE, chemical reaction and lower contact resistance.

The necessity of cooling the cold side of TEGs has been highlighted. Past experimental studies and the maximum efficiency achieved by different cooling methods in relation to the temperature difference indicated the importance of cooling. Various heat rejection techniques suitable for a wide range of power generation have been reviewed. Passive air cooling emerges as a suitable method for low power generation, while forced water cooling is suitable for industrial heat recovery despite its parasitic losses. Further research is required on hybrid cooling techniques and the minimization of parasitic losses. Finally, the feasibility of TEGs for implantable and wearable devices was discussed. The remarkable advantages of implantable TEGs in replacing batteries has been highlighted. Experimental studies on small animals show promising results for TEGs to be a potential long-term energy supplier and a possible alternative to batteries. The power requirements of common implantable devices are listed with a detailed case study on pacemakers. Equations pertaining to the design of TEGs for implantable and wearable sensors are provided. Further study is required on the biocompatibility of thermoelectric materials and any toxic effects on patients.

**Author Contributions:** Original draft preparation, P.M.K.; Review and editing, V.J.B., A.B., A.S.; Supervision, H.W., N.T., S.R.

**Funding:** This research was funded by a 2016 ASTAR AME IRG grant.

**Conflicts of Interest:** The authors declare no conflict of interest.

## References

- Gould, C.; Shammass, N.; Grainger, S.; Taylor, I. A comprehensive review of thermoelectric technology, micro-electrical and power generation properties. In Proceedings of the 26th International Conference on Microelectronics, Nis, Serbia & Montenegro, 11–14 May 2008; pp. 329–332.
- DiSalvo, F.J. Thermoelectric cooling and power generation. *Science* **1999**, *285*, 703–706. [[CrossRef](#)]
- Bottnner, H.; Nurnus, J.; Gavrikov, A.; Kuhner, G.; Jagle, M.; Kunzel, C.; Eberhard, D.; Plescher, G.; Schubert, A.; Schlereth, K.-H. New thermoelectric components using microsystem technologies. *J. Microelectromech. Syst.* **2004**, *13*, 414–420. [[CrossRef](#)]
- Snyder, G.J.; Soto, M.; Alley, R.; Koester, D.; Conner, B. Hot spot cooling using embedded thermoelectric coolers. In Proceedings of the Twenty-Second Annual IEEE Semiconductor Thermal Measurement and Management Symposium, Dallas, TX, USA, 14–16 March 2006; pp. 135–143.
- Rini, D.P.; Chow, L.; Anderson, H.R.; Kapat, J.S.; Carman, B.; Gulliver, B.; Recio, J.M. Method and Apparatus for Highly Efficient Compact Vapor Compression Cooling. U.S. Patent 7,010,936, 14 March 2006.
- O'Brien, R.; Ambrosi, R.; Bannister, N.; Howe, S.; Atkinson, H.V. Safe radioisotope thermoelectric generators and heat sources for space applications. *J. Nucl. Mater.* **2008**, *377*, 506–521. [[CrossRef](#)]
- Jung, K.K.; Jung, Y.; Choi, C.J.; Lee, J.M.; Ko, J.S. Flexible thermoelectric generator with polydimethyl siloxane in thermoelectric material and substrate. *Curr. Appl. Phys.* **2016**, *16*, 1442–1448. [[CrossRef](#)]
- Bell, L.E. Cooling, heating, generating power, and recovering waste heat with thermoelectric systems. *Science* **2008**, *321*, 1457–1461. [[CrossRef](#)] [[PubMed](#)]
- Tritt, T.M. Thermoelectric phenomena, materials, and applications. *Annu. Rev. Mater. Res.* **2011**, *41*, 433–448. [[CrossRef](#)]
- Shakouri, A. Recent developments in semiconductor thermoelectric physics and materials. *Annu. Rev. Mater. Res.* **2011**, *41*, 399–431. [[CrossRef](#)]
- Sootsman, J.R.; Chung, D.Y.; Kanatzidis, M.G. New and old concepts in thermoelectric materials. *Angew. Chem. Int. Ed.* **2009**, *48*, 8616–8639. [[CrossRef](#)] [[PubMed](#)]

12. Elsheikh, M.H.; Shnawah, D.A.; Sabri, M.F.M.; Said, S.B.M.; Hassan, M.H.; Bashir, M.B.A.; Mohamad, M. A review on thermoelectric renewable energy: Principle parameters that affect their performance. *Renew. Sustain. Energy Rev.* **2014**, *30*, 337–355. [[CrossRef](#)]
13. Riffat, S.B.; Ma, X. Thermoelectrics: A review of present and potential applications. *Appl. Therm. Eng.* **2003**, *23*, 913–935. [[CrossRef](#)]
14. Snyder, G.J.; Toberer, E.S. Complex thermoelectric materials. In *Materials for Sustainable Energy: A Collection of Peer-Reviewed Research and Review Articles from Nature Publishing Group*; World Scientific Publishing Co Pte Ltd: Hackensack, NJ, USA, 2011; pp. 101–110.
15. Chen, G.; Dresselhaus, M.; Dresselhaus, G.; Fleurial, J.-P.; Caillat, T. Recent developments in thermoelectric materials. *Int. Mater. Rev.* **2003**, *48*, 45–66. [[CrossRef](#)]
16. Komabayashi, M.; Hijikata, K.-I.; Ido, S. Effects of some additives on thermoelectric properties of FeSi<sub>2</sub> thin films. *Jpn. J. Appl. Phys.* **1991**, *30*, 331. [[CrossRef](#)]
17. Kuhling, K.; Graeser, M.; Wendorff, J.H.; Greiner, A. Thermoelectric Nanomaterials. U.S. Patent Application 12/159,408, 1 January 2009.
18. Zhao, L.-D.; Lo, S.-H.; Zhang, Y.; Sun, H.; Tan, G.; Uher, C.; Wolverton, C.; Dravid, V.P.; Kanatzidis, M.G. Ultralow thermal conductivity and high thermoelectric figure of merit in SnSe crystals. *Nature* **2014**, *508*, 373. [[CrossRef](#)]
19. Kanatzidis, M.G.; Hogan, T.; Mahanti, S. *Chemistry, Physics, and Materials Science of Thermoelectric Materials: Beyond Bismuth Telluride*; Springer Science & Business Media: Berlin, Germany, 2012.
20. Barako, M.; Park, W.; Marconnet, A.; Asheghi, M.; Goodson, K. Thermal cycling, mechanical degradation, and the effective figure of merit of a thermoelectric module. *J. Electron. Mater.* **2013**, *42*, 372–381. [[CrossRef](#)]
21. Zhang, G.; Zhang, Y.-W. Strain effects on thermoelectric properties of two-dimensional materials. *Mech. Mater.* **2015**, *91*, 382–398. [[CrossRef](#)]
22. Zhao, D.; Tian, C.; Liu, Y.; Zhan, C.; Chen, L. High temperature sublimation behavior of antimony in CoSb<sub>3</sub> thermoelectric material during thermal duration test. *J. Alloy. Compd.* **2011**, *509*, 3166–3171. [[CrossRef](#)]
23. Ren, F.; Wang, H.; Menchhofer, P.A.; Kiggans, J.O. Thermoelectric and mechanical properties of multi-walled carbon nanotube doped Bi<sub>0.4</sub>Sb<sub>1.6</sub>Te<sub>3</sub> thermoelectric material. *Appl. Phys. Lett.* **2013**, *103*, 221907. [[CrossRef](#)]
24. Ren, F.; Case, E.; Timm, E.; Schock, H. Hardness as a function of composition for n-type LAST thermoelectric material. *J. Alloy. Compd.* **2008**, *455*, 340–345. [[CrossRef](#)]
25. Dresselhaus, M.; Chen, G.; Ren, Z.; Dresselhaus, G.; Henry, A.; Fleurial, J.-P. New composite thermoelectric materials for energy harvesting applications. *JOM* **2009**, *61*, 86–90. [[CrossRef](#)]
26. Ravi, V.; Firdosy, S.; Caillat, T.; Brandon, E.; Van Der Walde, K.; Maricic, L.; Sayir, A. Thermal expansion studies of selected high-temperature thermoelectric materials. *J. Electron. Mater.* **2009**, *38*, 1433–1442. [[CrossRef](#)]
27. Rogl, G.; Grytsiv, A.; Gürth, M.; Tavassoli, A.; Ebner, C.; Wünschek, A.; Puchegger, S.; Soprunyuk, V.; Schranz, W.; Bauer, E. Mechanical properties of half-Heusler alloys. *Acta Mater.* **2016**, *107*, 178–195. [[CrossRef](#)]
28. Rogachev, M.; Pavlova, L.; Shtern, Y.I. Investigation of thermal linear expansion for nanostructured Si<sub>0.8</sub>Ge<sub>0.2</sub>P<sub>0.022</sub> in wide temperature range. *J. Phys. Conf. Ser.* **2016**, *741*, 012203. [[CrossRef](#)]
29. Thakur, S.; Dhindaw, B.; Hort, N.; Kainer, K. Some studies on the thermal-expansion behavior of c-fiber, SiC<sub>p</sub>, and *in-situ* Mg<sub>2</sub> Si-Reinforced AZ31 Mg alloy-Based hybrid composites. *Metall. Mater. Trans. A* **2004**, *35*, 1167–1176. [[CrossRef](#)]
30. Dai, D.; Zhou, Y.; Liu, J. Liquid metal based thermoelectric generation system for waste heat recovery. *Renew. Energy* **2011**, *36*, 3530–3536. [[CrossRef](#)]
31. Sander, M.S.; Sharifi, F. Thermoelectric Nanotube Arrays. U.S. Patent Application 11/444,016, 6 December 2007.
32. Schilz, J.; Riffel, M.; Pixius, K.; Meyer, H.-J. Synthesis of thermoelectric materials by mechanical alloying in planetary ball mills. *Powder Technol.* **1999**, *105*, 149–154. [[CrossRef](#)]
33. Fukuda, K.; Sato, Y.; Kajihara, T. Thermoelectric Semiconductor Material, Manufacture Process Therefor, and Method of Hot Forging Thermoelectric Module Using the Same. U.S. Patent 6,274,802, 14 August 2001.
34. Ur, S.-C.; Nash, P.; Kim, I.-H. Solid-state syntheses and properties of Zn<sub>4</sub>Sb<sub>3</sub> thermoelectric materials. *J. Alloy. Compd.* **2003**, *361*, 84–91. [[CrossRef](#)]

35. Yu, C.-B.; Gao, C.-F. Analysis of a circular arc-crack in thermoelectric media. In Proceedings of the 2016 Symposium on Piezoelectricity, Acoustic Waves, and Device Applications (SPAWDA), Xi'an, China, 21–24 October 2006; pp. 207–212.
36. Ghoshal, U.S. Enhanced Interface Thermoelectric Coolers Using Etched Thermoelectric Material Tips. U.S. Patent 6,608,250, 19 August 2003.
37. Cole, T. Thermoelectric energy conversion with solid electrolytes. *Science* **1983**, *221*, 915–920. [[CrossRef](#)]
38. Lowhorn, N.D.; Wong-Ng, W.; Lu, Z.-Q.; Martin, J.; Green, M.L.; Bonevich, J.E.; Thomas, E.L.; Dilley, N.R.; Sharp, J. Development of a Seebeck coefficient Standard Reference Material™. *J. Mater. Res.* **2011**, *26*, 1983–1992. [[CrossRef](#)]
39. Tsubota, T.; Ohtaki, M.; Eguchi, K.; Arai, H. Thermoelectric properties of Al-doped ZnO as a promising oxide material for high-temperature thermoelectric conversion. *J. Mater. Chem.* **1997**, *7*, 85–90. [[CrossRef](#)]
40. Yu, C.; Choi, K.; Yin, L.; Grunlan, J.C. Light-weight flexible carbon nanotube based organic composites with large thermoelectric power factors. *ACS Nano* **2011**, *5*, 7885–7892. [[CrossRef](#)]
41. Anatyshuk, L.; Knyshov, G.; Krykunov, O.; Kobylansky, R.; Tyumentsev, V.; Moskalyk, I. Thermoelectric Device «ALTEC-7012» for Human Head Cooling. *Nauka Ta Innovacii* **2016**, *12*, 60–67. [[CrossRef](#)]
42. Weber, J.; Potje-Kamloth, K.; Haase, F.; Detemple, P.; Völklein, F.; Doll, T. Coin-size coiled-up polymer foil thermoelectric power generator for wearable electronics. *Sens. Actuators A Phys.* **2006**, *132*, 325–330. [[CrossRef](#)]
43. Rojas, J.P.; Conchouso, D.; Arevalo, A.; Singh, D.; Foulds, I.G.; Hussain, M.M. based origami flexible and foldable thermoelectric nanogenerator. *Nano Energy* **2017**, *31*, 296–301. [[CrossRef](#)]
44. Jo, S.; Kim, M.; Kim, M.; Kim, Y. Flexible thermoelectric generator for human body heat energy harvesting. *Electron. Lett.* **2012**, *48*, 1. [[CrossRef](#)]
45. Schmitz, A.; Stiewe, C.; Müller, E. Preparation of ring-shaped thermoelectric legs from PbTe powders for tubular thermoelectric modules. *J. Electron. Mater.* **2013**, *42*, 1702–1706. [[CrossRef](#)]
46. Min, G.; Rowe, D.M. Ring-structured thermoelectric module. *Semicond. Sci. Technol.* **2007**, *22*, 880. [[CrossRef](#)]
47. Jovovic, V. *Thermoelectric Waste Heat Recovery Program for Passenger Vehicles*; Gentherm Incorporated: Azusa, CA, USA, 2015.
48. Uchida, K.; Ishida, M.; Kikkawa, T.; Kirihara, A.; Murakami, T.; Saitoh, E. Longitudinal spin Seebeck effect: From fundamentals to applications. *J. Phys. Condens. Matter* **2014**, *26*, 343202. [[CrossRef](#)]
49. Fateh, H.; Baker, C.A.; Hall, M.J.; Shi, L. High fidelity finite difference model for exploring multi-parameter thermoelectric generator design space. *Appl. Energy* **2014**, *129*, 373–383. [[CrossRef](#)]
50. Hodes, M. Optimal pellet geometries for thermoelectric power generation. *IEEE Trans. Compon. Packag. Technol.* **2010**, *33*, 307–318. [[CrossRef](#)]
51. Fabián-Mijangos, A.; Min, G.; Alvarez-Quintana, J. Enhanced performance thermoelectric module having asymmetrical legs. *Energy Convers. Manag.* **2017**, *148*, 1372–1381. [[CrossRef](#)]
52. Kishita, Y.; Ohishi, Y.; Uwasu, M.; Kuroda, M.; Takeda, H.; Hara, K. Evaluating the life cycle CO<sub>2</sub> emissions and costs of thermoelectric generators for passenger automobiles: A scenario analysis. *J. Clean. Prod.* **2016**, *126*, 607–619. [[CrossRef](#)]
53. Snyder, G.J.; Lim, J.R.; Huang, C.-K.; Fleurial, J.-P. Thermoelectric microdevice fabricated by a MEMS-like electrochemical process. *Nat. Mater.* **2003**, *2*, 528. [[CrossRef](#)]
54. Kao, P.-H.; Shih, P.-J.; Dai, C.-L.; Liu, M.-C. Fabrication and characterization of CMOS-MEMS thermoelectric micro generators. *Sensors* **2010**, *10*, 1315–1325. [[CrossRef](#)]
55. Glosch, H.; Ashauer, M.; Pfeiffer, U.; Lang, W. A thermoelectric converter for energy supply. *Sens. Actuators A Phys.* **1999**, *74*, 246–250. [[CrossRef](#)]
56. Zabarjadi, M. Heat Management in Thermoelectric Power Generators. *Sci. Rep.* **2016**, *6*, 20951. [[CrossRef](#)]
57. Jaworski, M.; Bednarczyk, M.; Czachor, M. Experimental investigation of thermoelectric generator (TEG) with PCM module. *Appl. Therm. Eng.* **2016**, *96*, 527–533. [[CrossRef](#)]
58. Rowe, D.M. Conversion Efficiency and Figure-of-Merit. In *CRC Handbook of Thermoelectrics*; CRC Press: Boca Raton, FL, USA, 1995; pp. 31–37.
59. Özdemir, A.E.; Köysal, Y.; Özbaş, E.; Atalay, T. The experimental design of solar heating thermoelectric generator with wind cooling chimney. *Energy Convers. Manag.* **2015**, *98*, 127–133. [[CrossRef](#)]
60. Wang, C.-C.; Hung, C.-I.; Chen, W.-H. Design of heat sink for improving the performance of thermoelectric generator using two-stage optimization. *Energy* **2012**, *39*, 236–245. [[CrossRef](#)]

61. Mastbergen, D.; Willson, B.; Joshi, S. Producing light from stoves using a thermoelectric generator. *Ethos* **2005**, *2005*.
62. Hsu, C.-T.; Yao, D.-J.; Ye, K.-J.; Yu, B. Renewable energy of waste heat recovery system for automobiles. *J. Renew. Sustain. Energy* **2010**, *2*, 013105. [[CrossRef](#)]
63. Lee, Y.G.; Kim, J.; Kang, M.S.; Baek, S.H.; Kim, S.K.; Lee, S.M.; Lee, J.; Hyun, D.B.; Ju, B.K.; Moon, S.E. Design and Experimental Investigation of Thermoelectric Generators for Wearable Applications. *Adv. Mater. Technol.* **2017**, *2*, 1600292. [[CrossRef](#)]
64. Lv, H.; Li, G.; Zheng, Y.; Hu, J.; Li, J. Compact water-cooled thermoelectric generator (TEG) based on a portable gas stove. *Energies* **2018**, *11*, 2231. [[CrossRef](#)]
65. Kiflemariam, R.; Lin, C.-X. Numerical simulation of integrated liquid cooling and thermoelectric generation for self-cooling of electronic devices. *Int. J. Therm. Sci.* **2015**, *94*, 193–203. [[CrossRef](#)]
66. Champier, D.; Bédécarrats, J.-P.; Kousksou, T.; Rivaletto, M.; Strub, F.; Pignolet, P. Study of a TE (thermoelectric) generator incorporated in a multifunction wood stove. *Energy* **2011**, *36*, 1518–1526. [[CrossRef](#)]
67. Sajid, M.; Hassan, I.; Rahman, A. An overview of cooling of thermoelectric devices. *Renew. Sustain. Energy Rev.* **2017**, *78*, 15–22. [[CrossRef](#)]
68. Singh, R.; Tundee, S.; Akbarzadeh, A. Electric power generation from solar pond using combined thermosyphon and thermoelectric modules. *Sol. Energy* **2011**, *85*, 371–378. [[CrossRef](#)]
69. Niu, X.; Yu, J.; Wang, S. Experimental study on low-temperature waste heat thermoelectric generator. *J. Power Sources* **2009**, *188*, 621–626. [[CrossRef](#)]
70. Yazawa, K.; Wong, V.K.; Shakouri, A. Thermal challenges on solar concentrated thermoelectric CHP systems. In Proceedings of the 13th InterSociety Conference on Thermal and Thermomechanical Phenomena in Electronic Systems, San Diego, CA, USA, 30 May–1 June 2012; pp. 1144–1150.
71. Fan, H.; Singh, R.; Akbarzadeh, A. Electric power generation from thermoelectric cells using a solar dish concentrator. *J. Electron. Mater.* **2011**, *40*, 1311–1320. [[CrossRef](#)]
72. Aranguren, P.; Astrain, D.; Martínez, A. Study of complete thermoelectric generator behavior including water-to-ambient heat dissipation on the cold side. *J. Electron. Mater.* **2014**, *43*, 2320–2330. [[CrossRef](#)]
73. Li, W.; Paul, M.; Siviter, J.; Montecucco, A.; Knox, A.; Sweet, T.; Min, G.; Baig, H.; Mallick, T.; Han, G. Thermal performance of two heat exchangers for thermoelectric generators. *Case Stud. Therm. Eng.* **2016**, *8*, 164–175. [[CrossRef](#)]
74. Nuwayhid, R.; Hamade, R. Design and testing of a locally made loop-type thermosyphonic heat sink for stove-top thermoelectric generators. *Renew. Energy* **2005**, *30*, 1101–1116. [[CrossRef](#)]
75. Djafar, Z.; Putra, N.; Koestoer, R.A. The utilization of heat pipe on cold surface of thermoelectric with low-temperature waste heat. *Appl. Mech. Mater.* **2013**, *302*, 410–415. [[CrossRef](#)]
76. He, W.; Su, Y.; Riffat, S.; Hou, J.; Ji, J. Parametrical analysis of the design and performance of a solar heat pipe thermoelectric generator unit. *Appl. Energy* **2011**, *88*, 5083–5089. [[CrossRef](#)]
77. Boonyasri, M.; Jamradloedluk, J.; Lertsatitthanakorn, C.; Therdyothin, A.; Soponronnarit, S. Increasing the Efficiency of a Thermoelectric Generator Using an Evaporative Cooling System. *J. Electron. Mater.* **2017**, *46*, 3043–3048. [[CrossRef](#)]
78. Espinosa, N.; Lazard, M.; Aixala, L.; Scherrer, H. Modeling a thermoelectric generator applied to diesel automotive heat recovery. *J. Electron. Mater.* **2010**, *39*, 1446–1455. [[CrossRef](#)]
79. Haggi, M.; Thurow, K.; Stoll, R. Wearable devices in medical internet of things: Scientific research and commercially available devices. *Healthc. Inform. Res.* **2017**, *23*, 4–15. [[CrossRef](#)] [[PubMed](#)]
80. Tsui, C.-Y.; Li, X.; Ki, W.-H. Energy harvesting and power delivery for implantable medical devices. *Found. Trends Electron. Des. Autom.* **2013**, *7*, 179–246. [[CrossRef](#)]
81. Spencer, W. A review of programmed insulin delivery systems. *IEEE Trans. Biomed. Eng.* **1981**, *28*, 237–251. [[CrossRef](#)]
82. Moss, A.J.; Hall, W.J.; Cannom, D.S.; Daubert, J.P.; Higgins, S.L.; Klein, H.; Levine, J.H.; Saksena, S.; Waldo, A.L.; Wilber, D. Improved survival with an implanted defibrillator in patients with coronary disease at high risk for ventricular arrhythmia. *N. Engl. J. Med.* **1996**, *335*, 1933–1940. [[CrossRef](#)]
83. Adams, T.P. Wireless Programmer/Repeater System for an Implanted Medical Device. U.S. Patent 5,383,915, 24 January 1995.
84. Schmidt, C.L.; Skarstad, P.M. The future of lithium and lithium-ion batteries in implantable medical devices. *J. Power Sources* **2001**, *97*, 742–746. [[CrossRef](#)]

85. Gollakota, S.; Hassanieh, H.; Ransford, B.; Katabi, D.; Fu, K. They can hear your heartbeats: Non-invasive security for implantable medical devices. In Proceedings of the ACM SIGCOMM Computer Communication Review, Toronto, ON, Canada, 15–19 August 2011; pp. 2–13.
86. Horiba, T.; Maeshima, T.; Matsumura, T.; Koseki, M.; Arai, J.; Muranaka, Y. Applications of high power density lithium ion batteries. *J. Power Sources* **2005**, *146*, 107–110. [[CrossRef](#)]
87. Diouf, B.; Pode, R. Potential of lithium-ion batteries in renewable energy. *Renew. Energy* **2015**, *76*, 375–380. [[CrossRef](#)]
88. Majeau-Bettez, G.; Hawkins, T.R.; Strømman, A.H. Life cycle environmental assessment of lithium-ion and nickel metal hydride batteries for plug-in hybrid and battery electric vehicles. *Environ. Sci. Technol.* **2011**, *45*, 4548–4554. [[CrossRef](#)]
89. Jaeger, J.; Deal, E., Jr.; Roberts, D.; McFadden, E., Jr. *Cold Air Inhalation, Esophageal Temperature and Lung Function in Exercising Humans*; Army Research Inst of Environmental Medicine: Natick, MA, USA, 1979.
90. Cohen, M.L. Measurement of the thermal properties of human skin. A review. *J. Investig. Dermatol.* **1977**, *69*, 333–338. [[CrossRef](#)]
91. Xuan, Y.; Roetzel, W. Bioheat equation of the human thermal system. *Chem. Eng. Technol. Ind. Chem. Plant Equip. Process Eng. Biotechnol.* **1997**, *20*, 268–276. [[CrossRef](#)]
92. Fiala, D.; Lomas, K.J.; Stohrer, M. A computer model of human thermoregulation for a wide range of environmental conditions: The passive system. *J. Appl. Physiol.* **1999**, *87*, 1957–1972. [[CrossRef](#)] [[PubMed](#)]
93. Ishida, Y.; Carroll, J.; Pollock, M.; Graves, J.; Leggett, S. Reliability of B-mode ultrasound for the measurement of body fat and muscle thickness. *Am. J. Hum. Biol.* **1992**, *4*, 511–520. [[CrossRef](#)]
94. Olivo, J.; Carrara, S.; De Micheli, G. Energy harvesting and remote powering for implantable biosensors. *IEEE Sens. J.* **2011**, *11*, 1573–1586. [[CrossRef](#)]
95. Parsonnet, V. Power sources for implantable cardiac pacemakers. *Chest* **1972**, *61*, 165–173. [[CrossRef](#)]
96. Mallela, V.S.; Ilankumaran, V.; Rao, N.S. Trends in cardiac pacemaker batteries. *Indian Pacing Electrophysiol. J.* **2004**, *4*, 201.
97. Bhatia, D.; Bairagi, S.; Goel, S.; Jangra, M. Pacemakers charging using body energy. *J. Pharm. Bioallied Sci.* **2010**, *2*, 51. [[CrossRef](#)]
98. Moontasir, H.; Ravigururajan, T.S. *Bio-Thermal Battery for ICDs*; Wichita State University: Wichita, KS, USA, 2006.
99. Choi, M.Y.; Choi, D.; Jin, M.J.; Kim, I.; Kim, S.H.; Choi, J.Y.; Lee, S.Y.; Kim, J.M.; Kim, S.W. Mechanically powered transparent flexible charge-generating nanodevices with piezoelectric ZnO nanorods. *Adv. Mater.* **2009**, *21*, 2185–2189. [[CrossRef](#)]
100. Kulkarni, P.; Öztürk, Y. Requirements and design spaces of mobile medical care. *Acm Sigmobility Mob. Comput. Commun. Rev.* **2007**, *11*, 12–30. [[CrossRef](#)]
101. Feng, D.; Jiang, C.; Lim, G.; Cimini, L.J.; Feng, G.; Li, G.Y. A survey of energy-efficient wireless communications. *IEEE Commun. Surv. Tutor.* **2013**, *15*, 167–178. [[CrossRef](#)]
102. Bronzino, J.D. Principles of electroencephalography. In *The Biomedical Engineering Handbook*; 1995; Volume 1.
103. Bos, R. *Self-Starting of a Small Urban Darrieus Rotor*; Delft University of Technology: Delft, The Netherlands, 2012.
104. Respiroics, P. VitalSense. Available online: <http://www.actigraphy.com/> (accessed on 2 February 2019).
105. Vivonoetics. Vivosense. Available online: <https://www.vivosense.com/> (accessed on 2 February 2019).
106. Tjiu, W.; Marnoto, T.; Mat, S.; Ruslan, M.H.; Sopian, K. Darrieus vertical axis wind turbine for power generation II: Challenges in HAWT and the opportunity of multi-megawatt Darrieus VAWT development. *Renew. Energy* **2015**, *75*, 560–571. [[CrossRef](#)]
107. Ward, J.; Eaton, J.; Hale, H. Losses in power transmission networks. *Electr. Eng.* **1950**, *69*, 451. [[CrossRef](#)]
108. Curone, D.; Secco, E.L.; Tognetti, A.; Loriga, G.; Dudnik, G.; Risatti, M.; Whyte, R.; Bonfiglio, A.; Magenes, G. Smart garments for emergency operators: The ProeTEX project. *IEEE Trans. Inf. Technol. Biomed.* **2010**, *14*, 694–701. [[CrossRef](#)]
109. Lee, D.; Haymes, E.M. Exercise duration and thermoregulatory responses after whole body precooling. *J. Appl. Physiol.* **1995**, *79*, 1971–1976. [[CrossRef](#)]
110. Torfs, T.; Leonov, V.; Van Hoof, C.; Gyselinckx, B. Body-heat powered autonomous pulse oximeter. In Proceedings of the 5th IEEE Sensors, Daegu, South Korea, 22–25 October 2006; pp. 427–430.

111. Leonov, V.; Vullers, R. Wearable thermoelectric generators for body-powered devices. *J. Electron. Mater.* **2009**, *38*, 1491–1498. [[CrossRef](#)]
112. Leonov, V. Energy harvesting for self-powered wearable devices. In *Wearable Monitoring Systems*; Springer: Berlin, Germany, 2011; pp. 27–49.
113. Torfs, T.; Leonov, V.; Yazicioglu, R.F.; Merken, P.; Van Hoof, C.; Vullers, R.J.; Gyselinckx, B. Wearable autonomous wireless electro-encephalography system fully powered by human body heat. In *Proceedings of the IEEE Sensors, Lecce, Italy, 26–29 October 2008*; pp. 1269–1272.
114. Suarez, F.; Nozariasbmarz, A.; Vashae, D.; Öztürk, M.C. Designing thermoelectric generators for self-powered wearable electronics. *Energy Environ. Sci.* **2016**, *9*, 2099–2113. [[CrossRef](#)]
115. Wang, Y.; Shi, Y.; Mei, D.; Chen, Z. Wearable thermoelectric generator for harvesting heat on the curved human wrist. *Appl. Energy* **2017**, *205*, 710–719. [[CrossRef](#)]
116. Proto, A.; Bibbo, D.; Cerny, M.; Vala, D.; Kasik, V.; Peter, L.; Conforto, S.; Schmid, M.; Penhaker, M. Thermal energy harvesting on the bodily surfaces of arms and legs through a wearable thermo-electric generator. *Sensors* **2018**, *18*, 1927. [[CrossRef](#)]



© 2019 by the authors. Licensee MDPI, Basel, Switzerland. This article is an open access article distributed under the terms and conditions of the Creative Commons Attribution (CC BY) license (<http://creativecommons.org/licenses/by/4.0/>).